2007

Optimization of a hydraulic mixing nozzle

Joshua Jacob Engelbrecht
Iowa State University

Optimization of a hydraulic mixing nozzle

by

Joshua Jacob Engelbrecht

A thesis submitted to the graduate faculty

in partial fulfillment of the requirements for the degree of

MASTER OF SCIENCE

Major: Mechanical Engineering

Program of Study Committee:
Kenneth Bryden, Major Professor
James Bernard
Brian Steward

Iowa State University

Ames, Iowa

2007

UMI Number: 1447498

ProQuest Information and Learning Company
300 North Zeeb Road
P.O. Box 1346
Ann Arbor, MI 48106-1346

TABLE OF CONTENTS

LIST OF FIGURES

ABSTRACT

In industry, mixing tanks are used to homogenize two or more different products that have been combined. This work investigates the use of graph-based evolutionary algorithms (GBEAs) coupled with computational fluid dynamics (CFD) to seek an enhanced design for a hydraulic mixing nozzle. This work also outlines a method for a numerical specification of a nozzle design and generation of a properly formulated CFD model to analyze it. The impact of choice of graph on the optimization process is examined using four different graphs: cycle, hypercube, toroid, and Peterson. Conclusions about the general type of nozzles designed by each graph type are included in order to identify the design strengths associated with each graph. This work provides insight into the considerations required to obtain more desirable performance from a mixing nozzle. Characteristics that influence jet distance and trajectory are reviewed. Some of these characteristics include the shape and size of horn used to guide the jet and the open entrainment area between the horn and the jet. The relative importance of each of these traits and which traits have the most significant impact on the quality of a given design are also explored. Suggestions for nozzle design are summarized. This information allows the most limiting factors of a tank mixing design to be mitigated to the largest extent possible.

This work illustrates that using magnification ratio or velocity alone does not result in an optimized design. These factors must be weighted to obtain a design that balances these factors for the geometry of fluid volume to be mixed. Additionally, this work shows that nozzle placement is perhaps more significant than nozzle design for optimum mixing with minimum power consumption.

CHAPTER 1

Introduction

In industry, mixing tanks are used to homogenize two or products that have been combined. Chemical and carrier solutions can be mixed and maintained in suspension in a tank using hydraulic mixing nozzles. These hydraulic mixing nozzles direct carrier solution flow from the piping system to the storage and mixing tank. This ensures sufficient fluid motion within the tank for mixing and suspension of the chemicals. Hydraulic mixing nozzles have several advantages over mechanical agitators:

- Lower installation cost since there is no mechanical mixing propeller in the tank. This eliminates the cost of the propeller and the separate shaft, bearings, and drive unit needed for it.
- The propeller is an additional concern when the tank must be cleaned. This is of particular concern if the tank is used for multiple products and contamination between loads is not acceptable.
- Hydraulic mixers have no moving parts. This increases reliability and reduces maintenance.

Optimization of hydraulic mixing is important to batch process designs that require the solution in the tank to be of uniform composition. Both nozzle design and nozzle placement in the tank affect the ultimate uniformity of the tank mixture, the time required to achieve it, and the energy needed for the process. Improvements in hydraulic mixing nozzle design will allow improved tank mixing effectiveness from each nozzle and enable a wide

range of nozzle configurations and solutions to be considered. For example, a smaller number of nozzles could be used to achieve an equivalent level of tank mixing.

A common type of hydraulic mixing nozzle in use today utilizes a high-speed fluid jet created by an orifice combined with a horn mounted around the jet. A representative nozzle is illustrated in Figure 1.

Fluid from a flow source, such as a pump, is supplied to the nozzle jet. The fluid passes through an open area, and then the horn directs the flow from the jet. This creates a venturi in the open area and causes the total flow exiting the nozzle to be several times greater than the volume supplied to the jet. Figure 2 displays a nozzle cross section. Figure 3 displays the related performance data for a typical nozzle widely used in industry.

Several manufacturers make nozzles of this type, and they are optimized for operation at a given flow rate and pressure common to the application for which they are designed. In this thesis, a simulation-based design methodology for designing an optimized water mixing nozzle is developed. The algorithm developed utilizes a detailed validated computational fluid dynamic (CFD) model to determine performance. Following a review of the data, a weighted combination of the average horn exit velocity and magnification

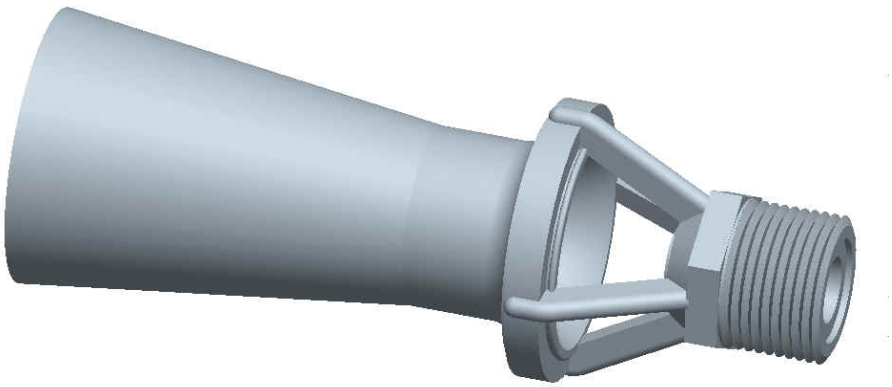

Figure 1. A typical mixing nozzle

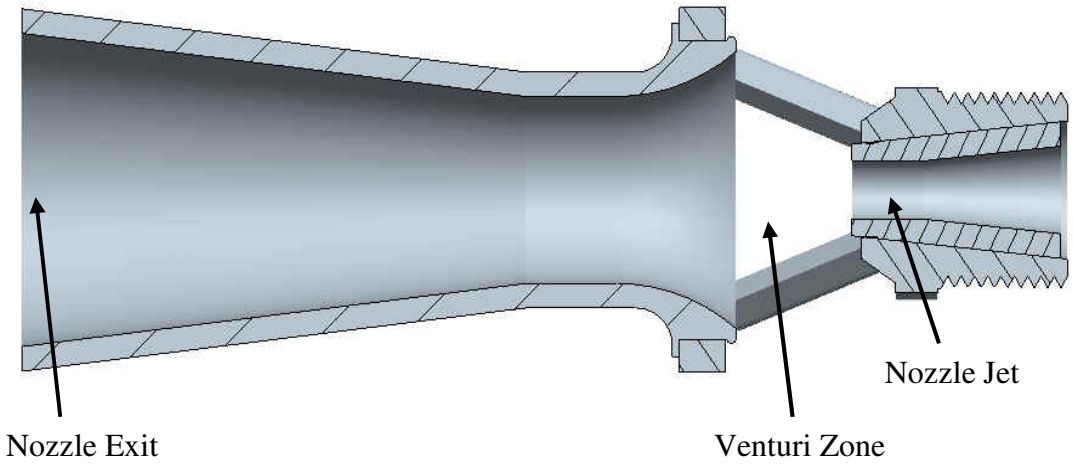

Figure 2. Cross section of a typical mixing nozzle

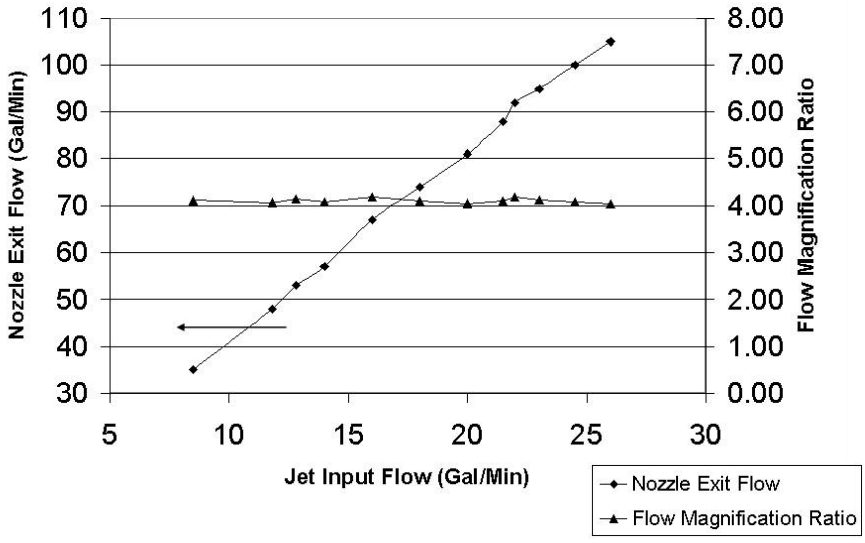

Figure 3. Nozzle flow performance of a typical mixing nozzle

ratio is used to determine the fitness of each nozzle design. Combining these factors seeks a design that is balanced between entraining significant volumes of fluid into the nozzle flow and maintaining sufficient velocity at the exit to create a velocity gradient to mix for a sufficient distance after the nozzle exit. Figure 4 outlines these parameters. CFD tools are used to simulate the performance of the nozzle. Graph based evolutionary algorithm (GBEA) tools [Bryden et al 2003] are used to manage the design evolution, development, and optimization.

In the following five sections, a detailed description of the nozzle design process is discussed. Section 2 presents the background section explaining the nozzle application and use. In Section 3 the computational model is developed. The computational model and its construction are reviewed in Section 3.1, the correlation with laboratory data explained in Section 3.2, and the grid study validation discussed in Section 3.3. Section 3.4 explains how a nozzle is characterized numerically to allow specification and measurement. The application of the evolutionary algorithm (EA) and fitness parameters are discussed in Section 3.5, and model management techniques are defined in Section 3.6. The model results are shared in Section 4. Conclusions and future work are summarized in Section 5.

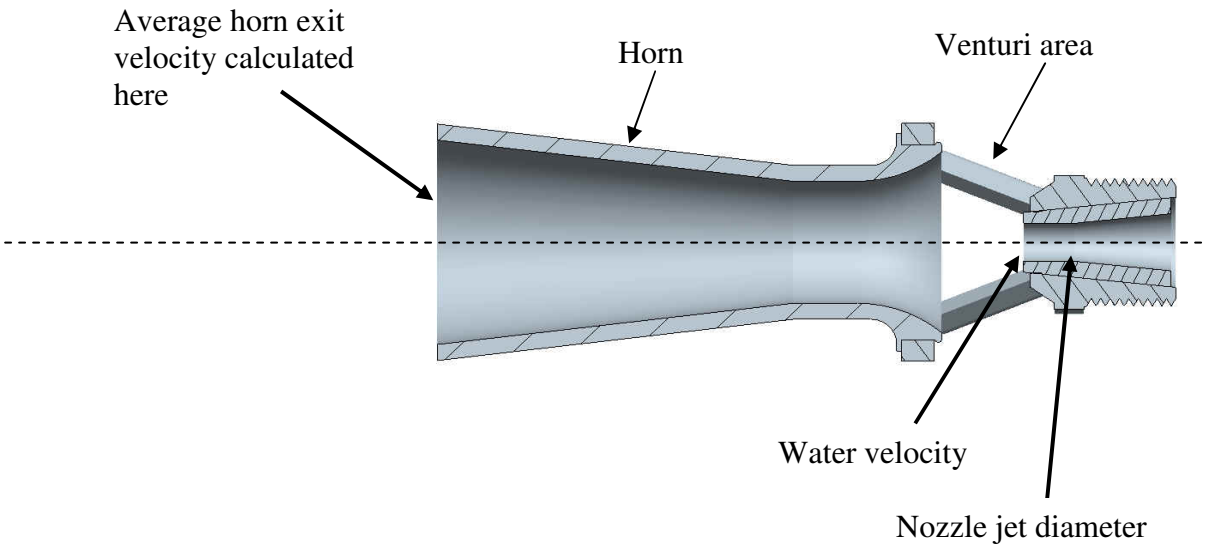

Figure 4. Key nozzle optimization parameters

CHAPTER 2

Background

Mixing chemicals in a tank is often required when a concentrated product is added to another carrier and the concentration of the mixed solution needs to be uniform. The batch process operations examined in this thesis consist of a tank for mixing and holding a chemical solution, and a pump to deliver this mixed solution to the next step in the process. This process is shown in Figure 5. When maintaining chemicals in solution by hydraulic mixing, a portion of the delivery pump's capacity is diverted from the main flow path back to the tank to drive the mixing nozzles. This diverted flow reduces the maximum capacity of the system to deliver the solution to the next stage of the process. Improved nozzle design could provide for several improvements:

1) If the flow from the pump required for mixing is reduced, the delivery capacity to the next process step is increased, allowing the cycle time for each batch to be reduced.
2) Alternately, a more efficient nozzle design allows the amount of flow currently diverted to the mixing nozzles to create a higher velocity gradient, creating a more vigorous mixing action, and maintain better mixing of the tank [Reynolds 1996].
3) Power needs of the pump may be reduced.

2.1 Nozzle Design

This chapter reviews current work in the areas of nozzle simulation and placement, mixing and jets, and jet pumps. Several authors have reviewed the number of jets and their

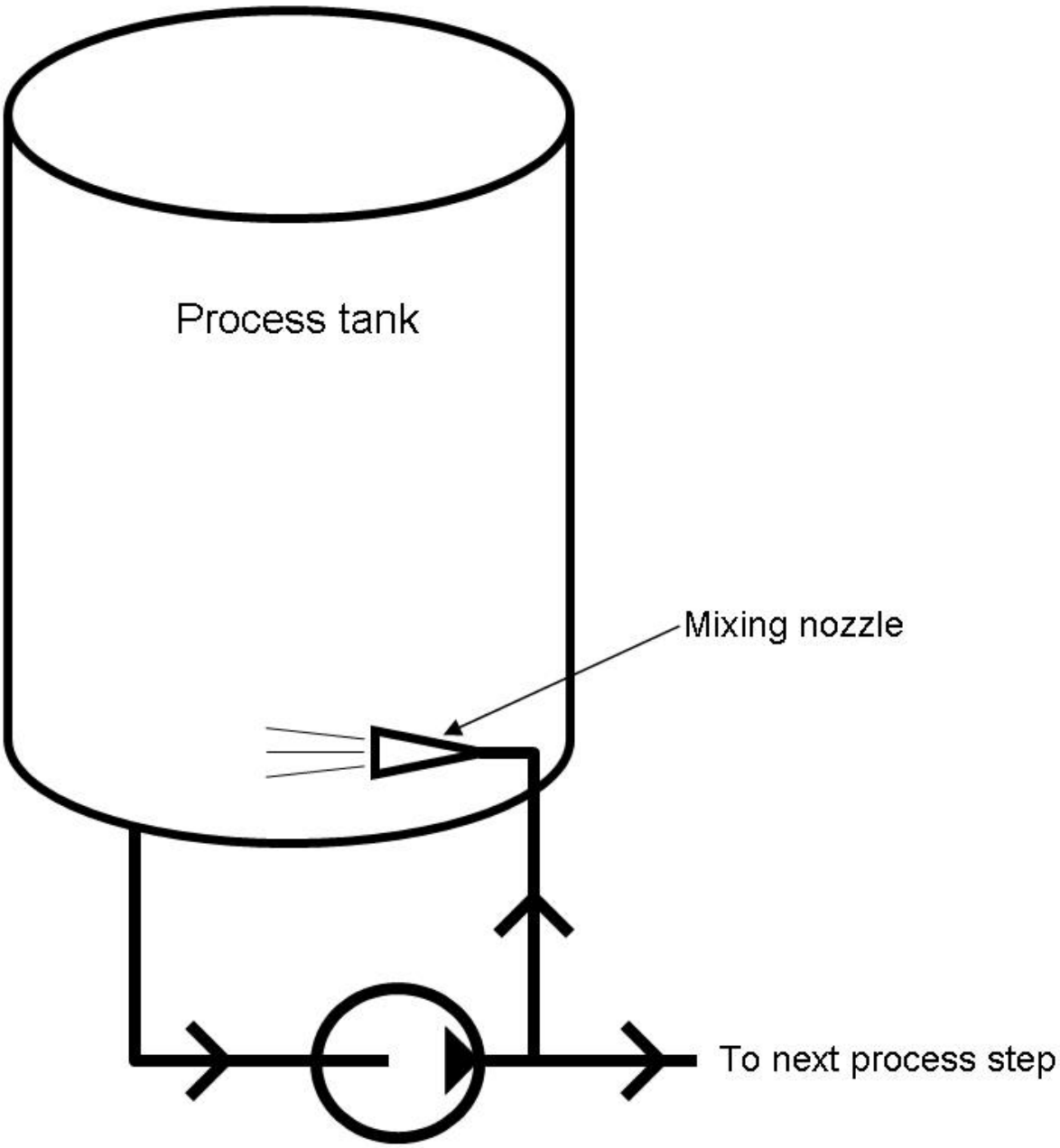

Figure 5. A batch process diagram

placement in a tank as they relate to a specific mixing configuration. Ucar et al [1998] propose a method for quantifying agitation using a physical turbidity measurement combined with concentration measurements for pesticide mixing in agricultural spraying tanks. They utilize both physical measurements and CFD simulations to determine effectiveness of nozzle placement patterns for the tank selected for their experiments. Ucar et al [2001] also correlate velocities measured throughout a hydraulically mixed tank with those computed with CFD. They are able to get most values to agree within 50%. Yates and Akesson [1963] also review the placement and number of nozzles in a sprayer tank and the level of mixing they create. Zughbi and Rakib [2004] also use CFD simulations to predict mixing in a jet-agitated tank based on nozzle placement.

Mixing is the combination of two or more liquids in the small eddies formed when a velocity gradient is created in the liquid. A turbulent jet is a column of fluid moving in a bulk fluid with a Reynolds number high enough to be considered turbulent. These jets create hydraulic mixing. Several authors have investigated comparisons between the physical models and the virtual computer models. Mann et al [1995] perform a comparative study of propeller mixing in a chemical batch tank. For two standard impeller geometries, they use tracers to investigate flow patterns and reagent segregation. They find a good match between the physical measurements and those predicted by the CFD model using a finite difference algorithm with a k-e turbulence model. Mann et al [1997] also draw similar conclusions in another propeller mixing experiment.

Hilgers and Boersma [2001] investigate effective ways to modify a jet of an incompressible fluid to improve mixing. They are able to create a flapping of a jet and

cause fast diffusion and mixing by applying helical and axial actuations at the orifice. They do not review any auxiliary guide apparatus.

Folsum [1948] and Gosline et al [1934] study water jet pumps. The geometry of the water jet pump looks similar to the reviewed nozzle. However, the results are largely preliminary, and are presented in light of suction lift and pumping against a back pressure, both of which are distinct differences in the design of a tank mixing nozzle.

Previous work related to horns used to increase mixing performance has emphasized nozzle placement related to a tank configuration [Ucar 1998, Yates and Akesson 1963, Zughbi and Rakib 2004], but not the nozzle design itself. Work reviewing nozzle design has emphasized diffusion at the maximum rate [Hilgers and Boersma 2001], with no consideration given to velocity at a distance from the jet. Velocity is an important factor to allow the nozzle to influence mixing in a greater portion of the tank by avoiding dissipation of the jet energy too quickly. In addition, the working length at the nozzle output needs to be related to tank size to ensure good mixing. Other authors have examined jet pumps with similar geometries, but emphasized different performance characteristics related to enhancing performance against backpressure, which is not present in the design of mixing nozzles.

2.2 Optimization in Design

The evolutionary algorithm techniques used in this study are based on the work of Bryden et al. [2003]. GBEAs utilize a graph to establish a geography for the population of evolving solutions. Each nozzle design is assigned to a node on the graphical structure. Any one node is permitted to share information only with other nodes to which it is connected on the graph. This controlled sharing allows a number of solutions to develop in the design

study. Geographically nearby nozzle designs can evolve quickly into effective performers. The limited interaction of geographically separated nozzles prevents designs that are promising, but not fully evolved, from being overwritten by nozzle designs that have already reached a higher performance level. This provides a chance for innovation that is not fully developed to survive. Each design can influence any other design, but this influence must propagate along a defined path. Four different graphical topologies are used in this project. A crossover and a mutation technique are also used to manage the development of nozzle solutions.

CHAPTER 3

Physical and Computational Model Description

The goal of this research is to define how to design an improved mixing nozzle. Understanding the aspects of the physical model and the computational model used to simulate it are both significant parts of the research. Section 3.1 describes the physical model in additional detail. Section 3.2 explains the computational model.

3.1 Physical Model Description

The baseline nozzle for this research is a plastic orifice with a venturi type horn fitted in front of the jet, as shown in Figure 1. This nozzle is commercially available. There is a gap between the jet and the start of the horn to allow fluid surrounding the nozzle to be entrained with the jet flow and carried through the end of the horn. This nozzle is injection molded from a non-corrosive polypropylene plastic. The orifice diameter is 7.9 mm (5/16”), the entrainment area has a length of 17.8 mm (0.7”), and the horn is 99 mm (3.9”) long.

Performance data obtained from physical testing are published by the manufacturer. Table 1 summarizes these published performance data. For this nozzle, the reported magnification ratio is approximately four. The magnification ratio is defined by the following formula:

$$m = f_t / f_j \qquad (1)$$

m = Magnification ratio
f_t = Total nozzle flow (jet and entrained flow)
f_j = Flow from nozzle jet

Table 1. Physical model performance data for a typical nozzle

Input Pressure (psi)	Input Flow (gal/min)	Output Flow (gal/min)	Magnification Ratio
10	8.5	35	4.12
20	11.8	48	4.07
25	12.8	53	4.14
30	14.0	57	4.07
40	16.0	67	4.19
50	18.0	74	4.11
60	20.0	81	4.05
70	21.5	88	4.09
75	22.0	92	4.18
80	23.0	95	4.13
90	24.5	100	4.08
100	26.0	105	4.04

The physical test data were collected by the manufacturer using the test system shown in Figure 6. Although the complete details of the manufacturer's testing process are not available, the general test procedure is as follows: A pump is connected to a tank filled with water, circulating through a valve to allowing the pump load to be adjusted. The nozzle is fitted in the bottom of the tank, and a two inch hose and flow meter are attached to the outlet of the nozzle. A pressure gauge is installed in the line supplying the nozzle. The pump is activated, and the valve is used to set the desired operating pressure. Total flow and velocity are then recorded. Based on experience, this test method overestimates the performance of the nozzle in practical applications, such as a mixing tank.

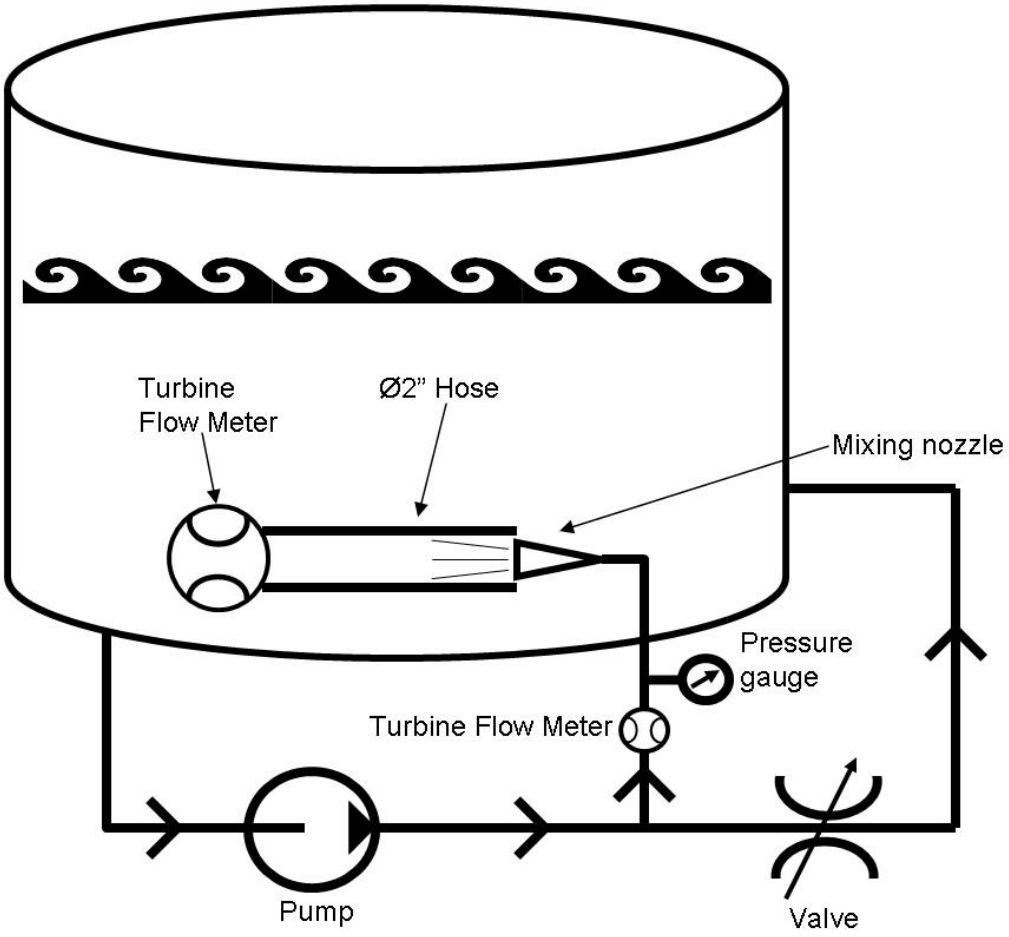

Figure 6. Test system to measure physical nozzle performance

3.2 Computational Model Description

To evaluate multiple nozzles using a CFD code, it is necessary to develop a grid with corresponding boundary conditions and solver parameters that would produce results consistent with the nozzle's physical performance, yet is still capable of calculating a solution in an amount of time that allows thousands of designs to be evaluated. To accomplish this, the first task is to model an existing mixing nozzle and compare the theoretical results to those measured in a test laboratory. Four grids are explored in order to develop a grid that produces satisfactory correlation to the lab results and allows for the testing of new nozzle geometries.

The CFD models are built and solved using STAR-CD™ 4.0. A number of grids and boundary conditions are explored to develop the final grid and parameters that are used for the design study. All grids use hexahedral cells. Extrusion layers are not used along the nozzle walls, but the cell size is kept small enough to properly reflect the conditions as the flow approaches the wall. Turbulence is modeled using the k-e high Reynolds number scheme with a turbulent intensity of 0.1 and entrance length of 0.0033 meters. The pressure relaxation factor is 0.35. This is determined by gradually increasing the factor until model convergence time no longer declines. The relaxation factors for momentum and KE turbulence were both 0.7.

In addition, the grid reduction technique is used to target the fine mesh resolution to areas of the flow field needing more accuracy. Teigland and Eliasson [2001] have investigated adding grid refinement to areas around model features expected to create turbulence or high velocity gradients in order to increase accuracy without large increases in computational time. Areas matching this description include segments of the model with

high fluid velocities and segments with large fluid velocity gradients at the jet exit and along the centerline axis of the nozzle. Larger cell sizes are used in areas of the flow field with less activity around the perimeter of the modeled cylinder. The nozzle geometry is also simplified to model only the horn used to guide the fluid flow. Small artifacts specific to the injection molding process are not included.

Several versions of the grid tested before selection of the final grid technique are summarized in Figures 6, 7, and 8. These are:

1) A 2-D grid of unit depth and nozzle cross section in the middle
2) A 2-D grid of unit depth and nozzle cross section in the corner
3) A pie shaped domain with cyclic boundaries
4) A cylindrical nozzle model

The first grid is a 2-D grid with unit depth. A cross-section of the nozzle is placed in the center of the domain. An inlet and outlet are placed behind the nozzle to simulate a pump, and symmetry planes are used on the faces of the cross section. This produces flows that yield a magnification of approximately two, which is only half of what was measured, and the domain necessary to remove the effects of recirculation caused by the pump flow is large and requires excess time to compute.

The second grid, shown in Figure 7, moves the nozzle cross-section to the corner of the 2-D domain. One side of the cross-section is removed and another symmetry condition is implemented. An inlet is applied at the jet, and a pressure boundary is used at the far end of the domain. Pressure boundaries are used instead of outlet boundaries so that the flow rate through the nozzle is not set by the boundary conditions. These boundary conditions correct the recirculation issues caused by the pump, but fluid enters and exits the model

across the same pressure boundary. This is not desired because of the potential numerical instability that it might cause. In addition, the magnification ratio is still too low, again approximately two. Clearly, a 3-D model is needed to accurately characterize the physical problem.

The third grid, with a wedge, or pie, shaped domain, is shown in Figure 8. The point of the wedge coincides with the centerline of the nozzle. To create the wedge, the cross-section of half the nozzle is created, and then swept through the angular direction to create the 3-D cells. To create the flat shells for the sweep, splines are used to outline the jet and the horn. The area between these features intended to be fluid is then filled with a series of patches of shells. The maximum size ratio permitted between adjacent patches is 2:1. Larger ratios do not perform well with STAR-CD™'s automated coupling features, which are used to establish cell connectivity in the mesh after the sweep. Small cell sizes are used close to the jet and through the entrainment zone to improve accuracy. Larger cell sizes are used at the opposite end of the domain away from the jet where the velocities are lower and flow direction more uniform.

The fluid domain represented by this model is a cylinder with a diameter of 254 mm (10") and a length of 914.4 mm (36"). The base of the nozzle is placed on a cylinder axis 127 mm (5") from the end. The nozzle points toward the far end, which is 787.4 mm (31") from the jet. This diameter is selected by testing successively larger diameter cylinders until further increases in diameter no longer change the results of the validation cases. The length of 787.4 mm (31") is selected based on tank sizes and shapes appropriate for the currently manufactured nozzle. The angle of the wedge is computed based on the cell size near the

radial axis. The angle is set to maintain a reasonable aspect ratio of the cells in this significant part of the model.

Cyclic boundary conditions are used on wedge faces, and pressure boundaries are used on the cylinder ends. This increases the accuracy of the results, increasing the magnification ratio to about three. However, flow separation from the centerline is observed just after the fluid exits the nozzle. This separation is not consistent with physical principles and is present for ¼ and 1/8 nozzle wedges. Using a grid with a ½ nozzle and symmetry plane, or a whole nozzle, shown in Figure 9, does not show this separation. This calls into question the use of cyclic boundary conditions for this application.

To verify that the pressure boundaries are not creating the incorrect flow pattern or prolonging the convergence time, boundary conditions of only inlets and outlets are tested. The wedge end adjacent to the nozzle inlet is set to a very low speed, and an outlet is applied to the boundary after the nozzle exit. However, the boundary flow does not allow the flow through the nozzle to properly develop and prevents the model from showing the flow action of the venturi.

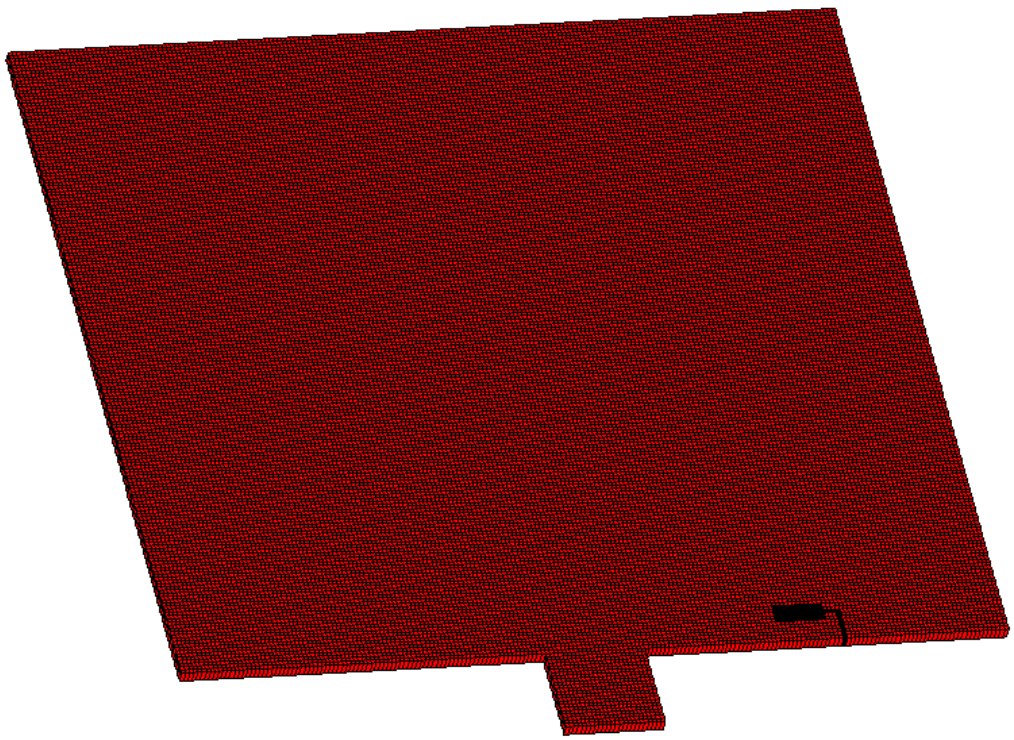

Figure 7. A 2-D grid of unit depth with
a nozzle cross-section in the corner

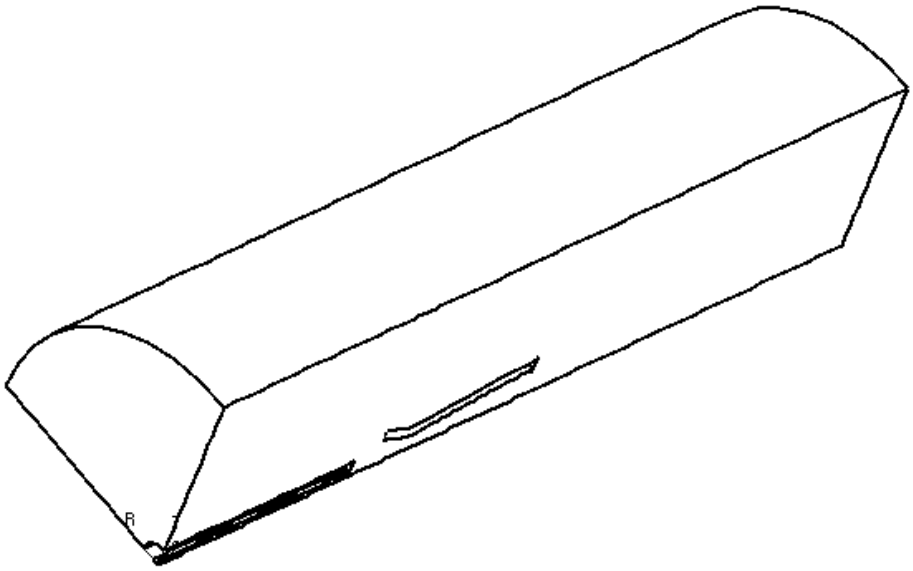

Figure 8. A ¼ nozzle model using
cyclic boundary conditions

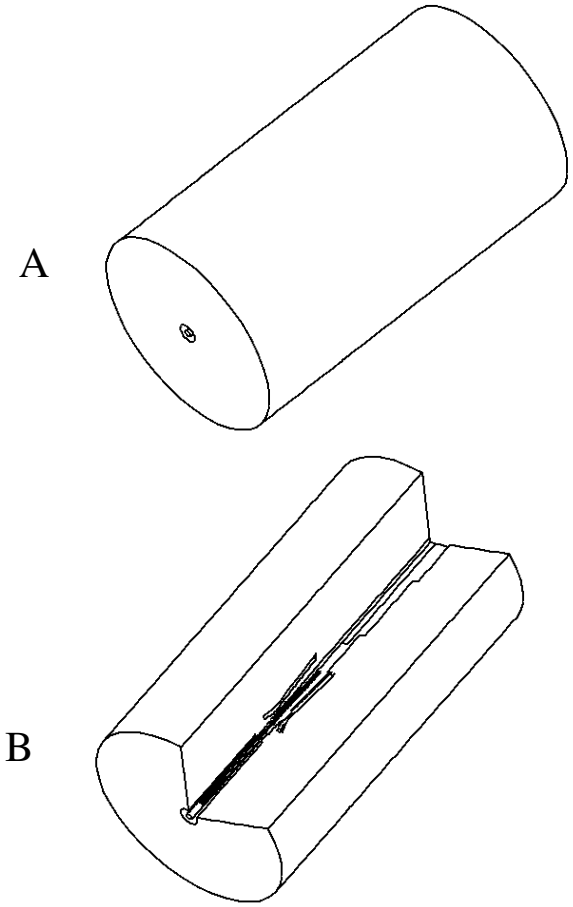

Figure 9. A whole nozzle model, A. entire, B. sectioned

Another wedge is created with a thickness of one cell. The angle of the wedge is adjusted based on cell size near the axis to keep the aspect ratio within acceptable limits. This varying angle is considered in all flow calculations such that the flows reported from the model are scaled to represent a complete nozzle. Symmetry planes are applied to the wedge faces, and the same inlet and pressure boundaries are applied to the wedge ends. This grid yields results that coincide within 2% of the data from the grid study. The flow exiting the nozzle no longer displays the centerline separation. Flow does not change directions across the boundaries, and the flow travels in the expected directions. The attributes of this grid, shown in Figure 10, are used for the subsequent grids used in the study.

In addition to the geometry in Figure 10, the final model uses a k-e high Reynolds number turbulence model with a turbulent intensity of 0.1. The entrance length is 0.0033 m, and the pressure factor is 0.35. The relaxation factors used for momentum and KE turbulence are 0.7. The models contain approximately 30,000 fluid cells for this work. The angle of the wedge is set based on the size of the cells near the centerline to maintain their aspect ratio. All the models are run using a jet exit speed of 18.3 m/s (60 ft/s).

Several variations of model parameters are tested to explore options in the solution space. Cases are run to explore solutions with similar characteristics to the manufactured nozzle to determine if a better design could be created using the same envelope. Cases are also run with greater freedom for all design variables to search for more abstract designs that may also prove to be good solutions.

More abstract cases are also run that give the model more dimensional freedom. The entrainment length was allowed to vary from 5.1 mm (0.2”) to 101.6 mm (4.0”). The horn

inside diameter is permitted to range from 25.4 mm (1.0”) to 76.2 mm (3.0”). The horn length is allowed to vary from 76.2 mm (3.0”) to 203.2 mm (8.0”). These general dimensions are selected based on knowledge and assumptions of the manufacturing techniques and typical installation locations for mixing nozzles of this type.

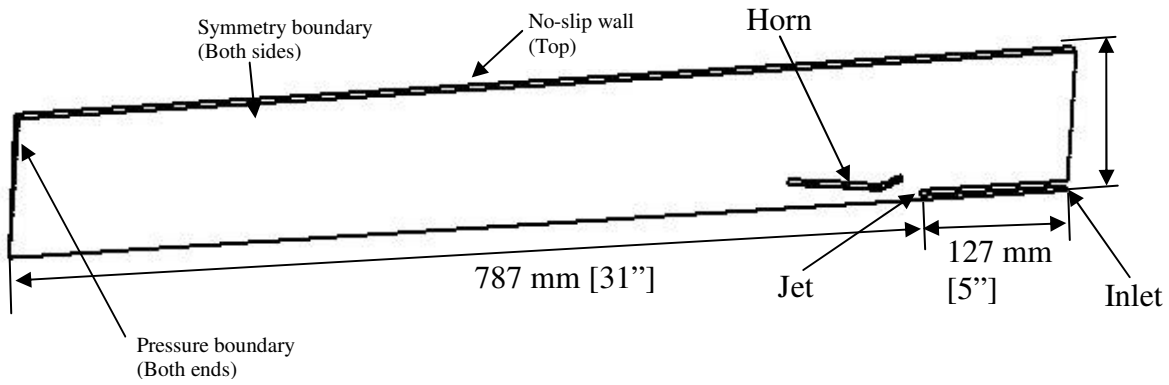

Figure 10. Computational grid

3.3 Model Validation

The computational model is validated by comparing it to laboratory test data. The currently manufactured nozzle is modeled using the grid parameters described above. The laboratory test consists of placing the manufactured design into a tank. A hose is connected over the end of the horn, and that flow is directed through a flow meter. The flow supplied to the nozzle jet is also measured with a flow meter. A pressure sensor indicates that back pressure on the nozzle created by the flow meter is negligible, less than 3.45 kPa (0.5 psi). The inlet flow from the jet in the model is set to match the inlet flow meter reading from the test, which is 18.1 m/s (59.5 ft/s). At this flow, the manufactured nozzle has an input pressure of 207 kPa (30 psi). When this is done, the model flow out of the horn correlates closely with the flow measured during the experiment. Table 2 compares the computed and laboratory data. There are some differences between the laboratory and model data, but several factors must be considered. The nozzle flow in the test is impacted by the added hose and flow measuring device. Calibration and accuracy limitations also exist with the physical test equipment.

Table 2: Computed nozzle performance vs. lab performance of a typical nozzle

	Lab	**Computed**	**Difference**
Magnification ratio	4.19	3.88	-7.5%
Velocity (m/s)	2.95	2.21	-25%

3.4 Grid Study

The CFD calculations for the nozzle evaluation consume most of the time required for the evaluation. Approximately 94% of the computational time used is consumed by CFD calculations and 6% of the time is used to create the mesh. Engineers typically invest most of the computer time in performing calculations with the hope that higher fidelity models will provide more insight and understanding of the design problems and physical phenomena governing the situation. In choosing the level of detail contained in the model, the engineer must consider the computational time required, and balance that with the level of fidelity necessary in the grid to obtain the desired answer, considering the amount of acceptable error in the model calculations. This level of fidelity must also allow for generation of a diverse set of designs. This constraint implies that the grid must still be able to maintain fidelity in the model regions required to maintain reasonable margins of error. However, evolutionary algorithms (EA) do not need to understand the physics governing the problem. An EA only "learns" which characteristics of the design result in the best optimization of the fitness criteria. Because of this, the EA requires a model with only enough detail to reliably determine which designs are better than others. Since the higher resolution grid matches experimental data that is collected in the lab, the EA only requires the lowest resolution grid with a solution that reasonably matches that of the high resolution grid. A grid study is used to determine what resolution is required for this model. Figure 11 graphically summarizes the results of the grid study.

Thirty-three grids with the geometry of the commercially available nozzle are tested, ranging from 958 to 146,543 cells. The accuracy of each grid is determined by reviewing two errors. One error is the absolute percent difference in the fitness value

between the grid under review and the finest grid. The other error is the absolute percent difference in magnification ratio between the grid under review and the finest grid. The first measure is to ensure there will be no unexpected impacts to the fitness criteria, and the second measure reflects error relative to the measured experimental data. Both error measurements track closely together, which supports the conclusion that the fitness criterion does not become detached from the model performance across the range of grid sizes.

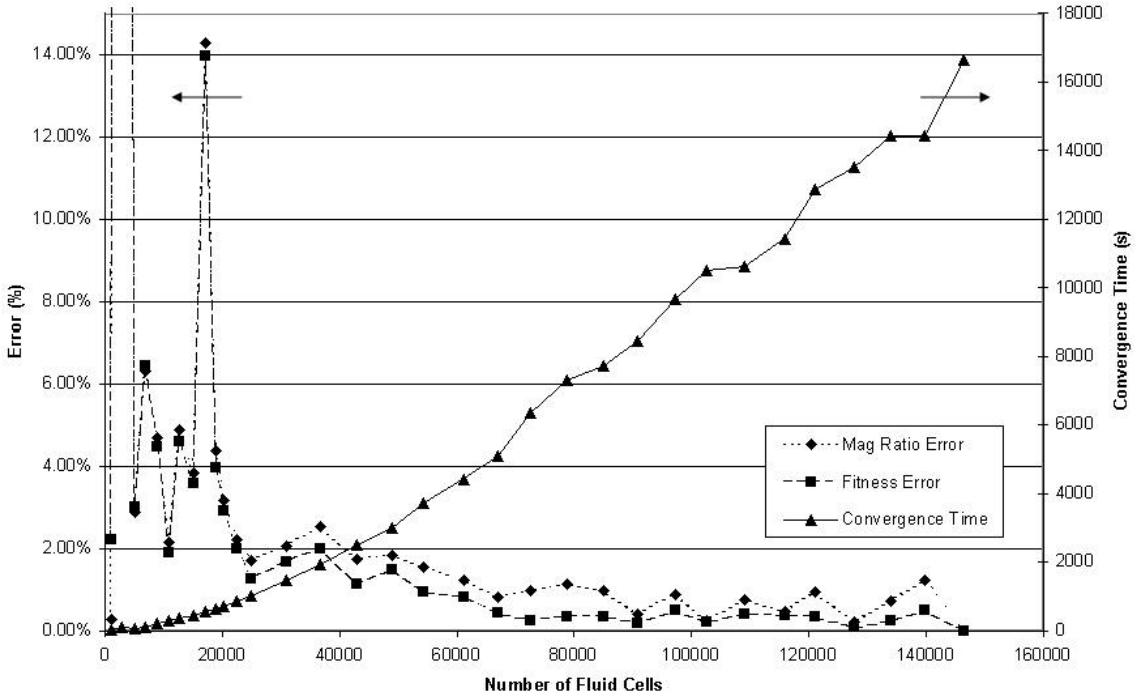

Figure 11. Grid study. Percent error and convergence time vs. number of fluid cells are shown. Errors decrease with additional cells, but computational time increases.

Figure 12 shows a selection of the errors and convergence time for each of the grids. Review of the graph shows significant oscillations in the errors between zero and 30,000 cells. Examination of the flow fields of the solutions show that recirculation regions around the jet and the horn entrance and exit appear and disappear as the number of cells changes in this area. The large changes in the error illustrate that properly representing these areas in the model is important to the solution.

Four images are shown in Figure 13 to illustrate the changing recirculation regions. The images on the left are from a grid of 17,000 fluid cells. The images on the right are from a grid of 15,000 fluid cells. Each row shows the same model region in each grid. Some of the differences in the flow field are highlighted by the circles. When selecting the number of cells to use for the EA model, it is important to select a cell count higher than this oscillating area. Mesh sizes below that cell count become accurate for specific geometries only, and cannot be applied generally to the variety of nozzle shapes reviewed by the algorithm.

Model performance has high variability in the region below 30,000 cells. Figure 14 illustrates two very similar nozzle profiles that are modeled with approximately 7000 cells. Nozzle 33 has a computed velocity of 2.26 m/s, while nozzle 34 has a computed velocity of only 0.76 m/s. The geometry of the two nozzles is very similar, but the differences in the formation of recirculation regions cause the results to be very different. Figure 15 illustrates the difference in size of the speed of the flow exiting the nozzle at this low cell density. Refining the two grids to contain a higher number of cells causes the results to agree very closely. This example is another illustration of volatility in the lower cell count grids.

Although the percent error is lower on the grid study at this specific point, the recirculation regions in other geometries with small changes are calculated in very different ways.

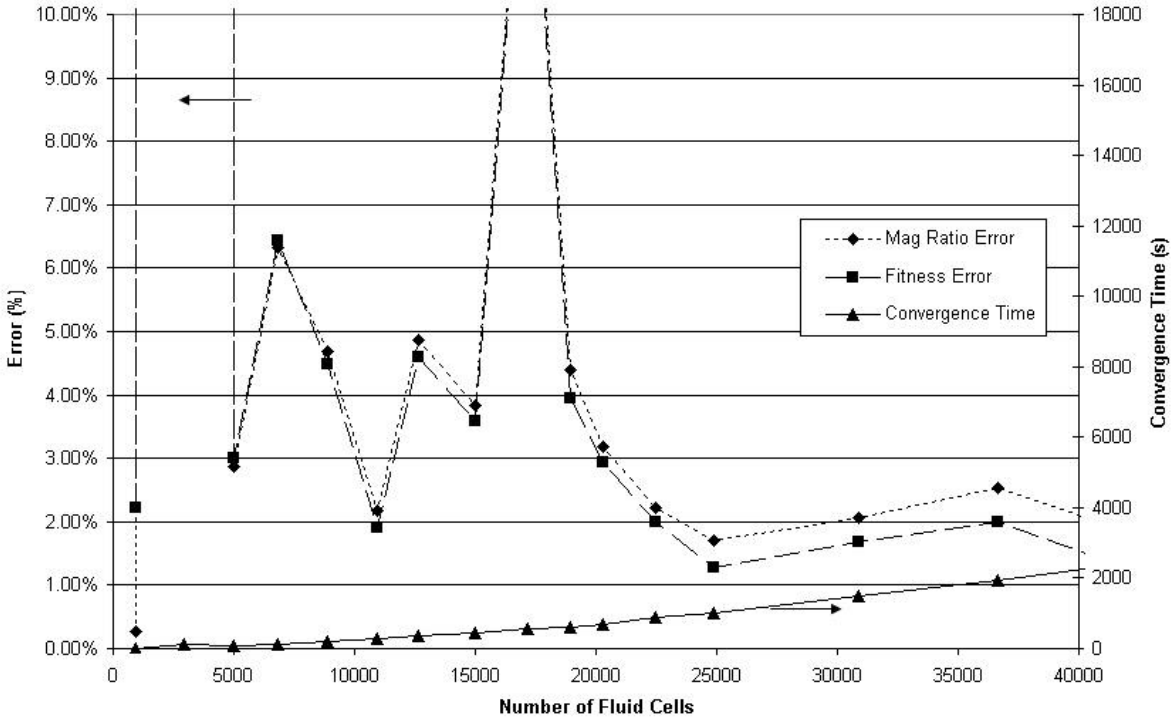

Figure 12. Detailed portion of Figure 11. Error oscillates significantly when the number of fluid cells drops below 25,000.

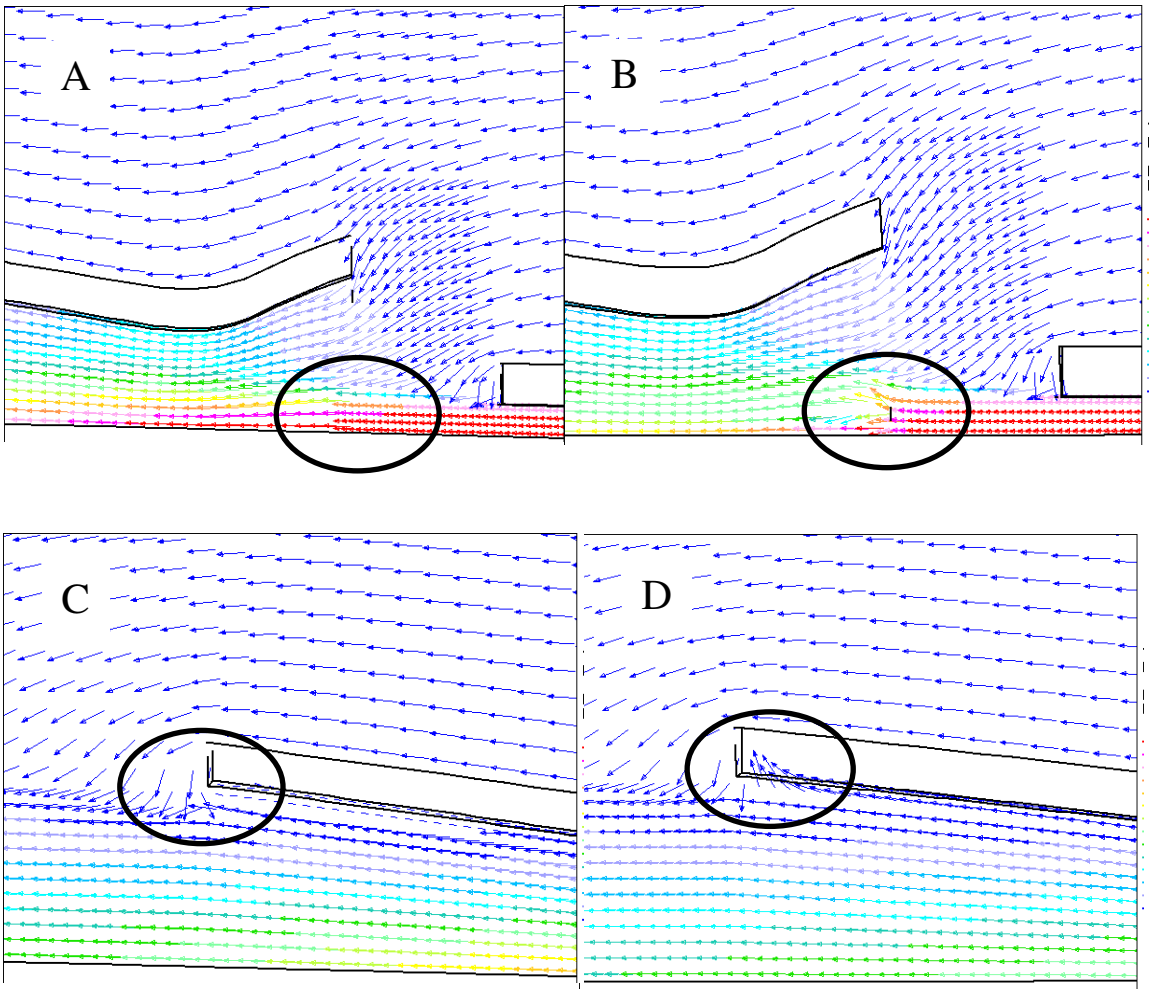

Figure 13. Comparison of two grid densities from the typical nozzle. A and C highlight two portions of a grid containing 17,000 cells. B and D highlight the same portions of a grid containing 15,000 cells. Note the changes in circulation patterns as the grid density changes.

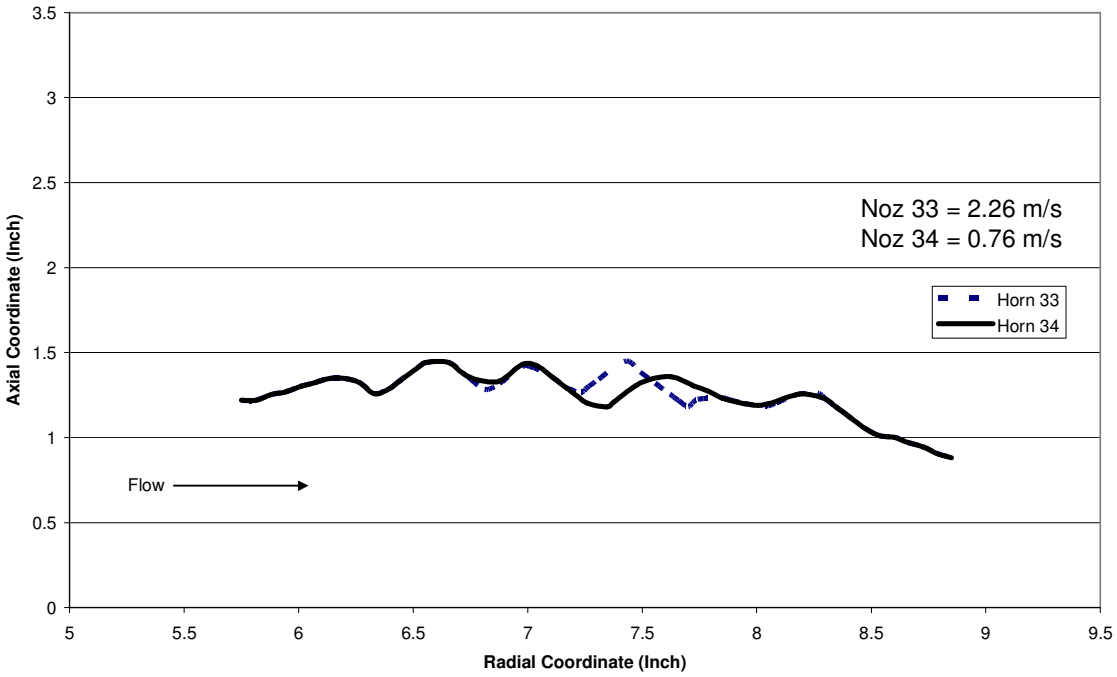

Figure 14. Comparison of nozzle profiles from nozzles 33 and 34. The profiles differ only slightly in the middle, but there is a significant difference in the nozzle flow velocity at a grid density of approximately 7000 cells.

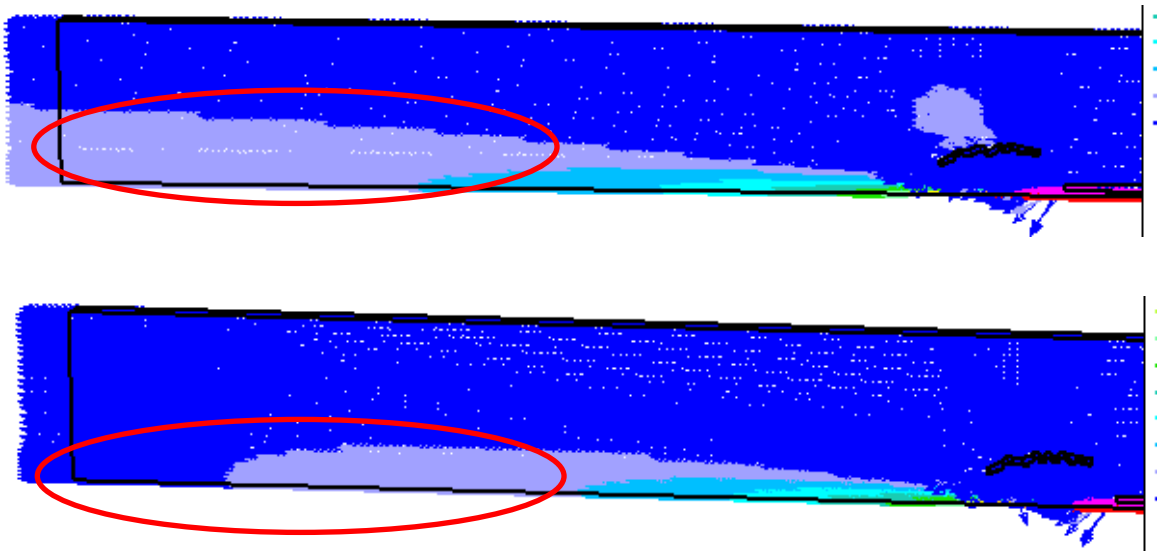

Figure 15. Comparison of jets from nozzles 33 and 34. The jet from nozzle 33, in the upper view, is larger and of higher speed than the jet of nozzle 34, in the lower view.

The volatile area of the grid study below 30,000 cells shows this design problem is very sensitive to the grid's ability to resolve critical features. Because the nozzle model can become erratic at low cell counts, reducing the number of cells below this threshold is not practical. This finding is in contrast to Figure 5 in Bryden et al [2003], which illustrates a grid study performed on a plancha stove. This grid study shows a generally smooth increase in error as cell count is reduced. No erratic or unpredictable models are shown as the computational model is made coarser. This case is less sensitive to finer fluid phenomena in grid. The stove models do not perform erratically at lower cell counts, and this allows the use of a lower cell count model to be an effective way to reduce computational requirements to solve the problem. However, in the nozzle model the grid must resolve some critical details, so it cannot be made continually coarser to reduce the computational time required for convergence because model accuracy becomes completely unpredictable. Other ideas to improve computational performance must be explored.

Grid selection is based on comparison between speed and accuracy. A combination of cell sizes creating about 30,000 cells per model is selected for this work. This point occurs before the computation time becomes very long, but after volatility of the lower cell counts.

3.5 Nozzle Construction

The nozzle construction is characterized by several dimensions to allow nozzle construction and shape variation by the GBEA routine. These parameters are subsequently used to assemble a CFD model that can accommodate design variation as nozzle designs are reviewed. Proper attributes and settings are selected based on results from a grid study. These models are combined with combinatorial graphs to manage and develop the nozzle

design. This process allows the engineer to generate multiple high quality designs from which to choose. A diversity of design alternatives permits the engineer greater latitude to consider secondary factors and exercise engineering judgment to address the issues related to creating better mixing technology. A diversity of solutions also permits the engineer to improve his or her intuition about what characteristics are important to the design of the nozzle. The characteristics and techniques to generate multiple designs for the nozzle will be discussed throughout the rest of the paper.

The nozzles to be designed can be described by six parameters. The parameters, shown in Figure 16, are:

1. Length- This defines the axial length of the plastic horn placed in front of the jet
2. Entrainment length- This defines the axial distance from the jet to the beginning of the horn
3. Number of inflection points- Nozzle shapes could be concave or convex. This parameter sets the number of times the slope of the horn changes with respect to the axial direction
4. Location of inflections points- This defines the distance of each inflection point from the beginning of the horn
5. Starting direction- This defines whether the initial horn slope will be convex or concave
6. Initial diameter- This sets the initial diameter of the horn at its base, the end closest to the nozzle jet

Fifty points are created to define each horn. Only a sample of points is shown in Figure 16 for clarity. The points are evenly spaced in the axial direction along the length of the horn.

The radial coordinate of the first point is defined based on the initial diameter parameter. A random offset from the first point is generated to determine the radial coordinate of the second point. The magnitude of the offset is limited such that the slope of the horn wall cannot exceed 45 degrees. The direction the offset is applied is determined by the starting direction parameter. The offset is not applied if it would cause the radial coordinate to fall outside the maximum or minimum horn diameter limits. When an inflection point is reached, the application direction of the offset is reversed.

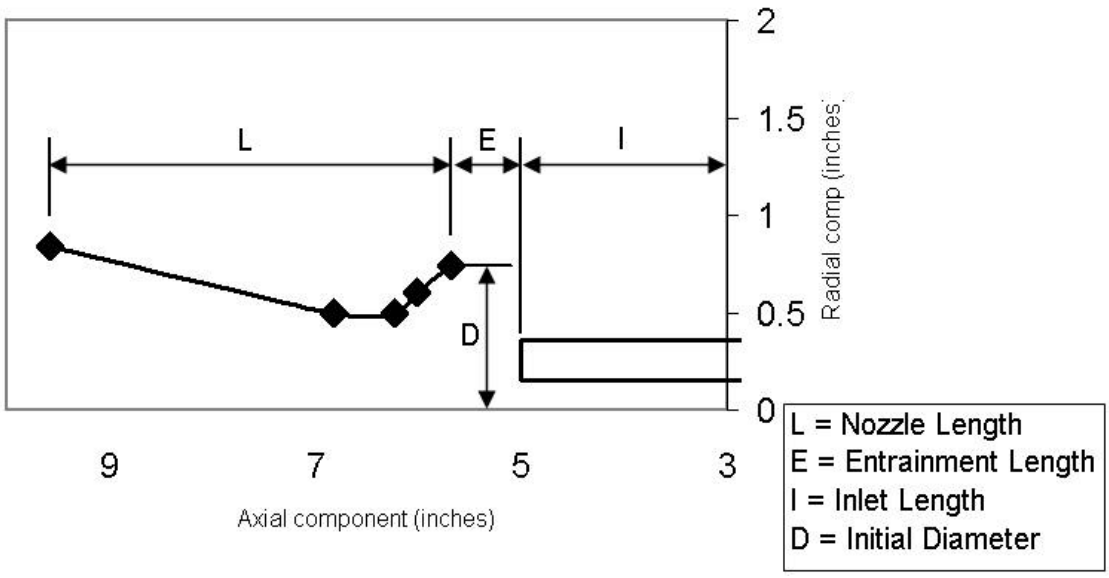

Figure 16. Nozzle optimization dimensions. These dimensions are used to generate new nozzles and numerically summarize nozzles created during mating events.

3.6 Evolutionary Algorithm

One of the pitfalls of evolutionary computation is the potential for premature convergence of the algorithm to an inferior design. There are computationally expensive methods of preventing premature convergence, such as restarting the algorithm or niche specialization [Mitchell 1998]. Graph-based evolutionary algorithms [Bryden 2005] provide an alternative method of avoiding premature convergence. Members of an evolving population are placed on the vertices of a combinatorial graph; this has the effect of placing a geographic structure on the population. Different areas of the geographic structure have subpopulations that explore different parts of the search space.

Premature convergence is still possible, but less likely because the algorithm explores many areas and hence has more chances to avoid the local optima of the search space that are the cause of premature convergence. The geography imposed on the population thus yields many of the same benefits as restarting or niche specialization while avoiding their computational cost. The computational cost of using a graph-based algorithm is only the cost of maintaining the connectivity of the geography and referring to it--a very low cost indexing operation.

The price of using graph-based algorithms is that the correct graph must be chosen. Experiments suggest that the correct graph is a sparse one for difficult or polymodal problems and a highly connected one for simple or unimodal problems [Bryden 2005]. An ongoing effort to classify problems by their interaction with graphs [Ashlock 2006] seeks to make the selection of graphs more exact.

The graph-based evolutionary algorithms based on the work of Bryden et al [2003] are used for this research. Using this work requires development of a method for a crossover operation and a method for a mutation operation. A population of sixty-four nozzles is used in this genetic algorithm implementation. The cycle, hypercube, toroid, and Peterson families of graphs are each tested in this work. Each graph run consists of 2000 mating events.

One fitness criterion considered and rejected for this work is the peak velocity of the liquid across a plane perpendicular to the nozzle axis located 787.4 mm (31") from the jet. The distance is selected based on typical sizes of tanks for the target market. Experiments considering velocity alone generate nozzles that are very long and narrow. In essence, they are shaped in such a way that the effect is to extend the jet pipe down the domain as close as possible to the model exit. Peak exit velocity is high, but fluid movement and velocity gradient in the main volume of the model is small. This design causes high loss of energy and is not conducive to practices used to manufacture these devices.

A second criterion considered and rejected for determining fitness is the average velocity across the exit of the horn. Using this fitness criterion yields designs that have a more practical appearance than the first criterion. However, the nozzles have inlet geometries that hinder overall performance, and the nozzles still have a general appearance of being long and narrow, along with extended entrainment lengths.

A third criterion considered and rejected for determining design fitness is the magnification ratio of the nozzle. The magnification ratio is the total flow exiting the nozzle horn divided by the total flow supplied to the jet by the pump. Using this fitness measure encourages nozzle designs with large diameter horns that are very cylindrical. This creates

the maximum possible area for measuring exit flow, and inflates the fitness measure. Most mixing nozzles currently manufactured are promoted using this measure of efficiency, but it does not prove to be a reliable measurement of fitness for mixing nozzles.

The fitness criterion selected is a combination of the second and third values described above. While neither value alone is a sufficient measure of fitness, together they create a balanced design criterion for the nozzle. Each of the values above is normalized by an expected maximum value and summed together. The final formula for nozzle fitness is:

$$f = \frac{m}{10} + \frac{v}{5} \tag{2}$$

Where f is the fitness of the model, m is the magnification ratio, and v is the average fluid velocity (m/s) exiting the horn. The divisors are selected based on potential maximum values for each trait and data collected from models computed in the course of this work. Combining the two values encourages higher speeds to obtain larger velocity gradients while balancing the other requirement of moving mass throughout the fluid.

3.7 Other Model Management Techniques

Two major computational issues are noted while performing this research. The first computational issue is nozzles that will not converge, or that converge very slowly. Examination of these nozzles reveals they typically have extreme geometry that would not make a good design solution, and this extreme geometry creates anomalies in the flow field that the solver cannot resolve without significantly more grid. To resolve this, if a solution calculation exceeds 5000 iterations, the calculation is stopped and the nozzle is mutated. This serves as a penalty function to the EA to discourage geometry that is not suitable.

The second computational issue is excess fluid velocity. With some infeasible extreme nozzle geometries, the pressure boundary conditions allow the solver to find a solution where the velocity in the main part of the flow field exceeds the input velocity at the jet, which is not physically possible. To stop the solver from creating these solutions, the calculations are stopped and the nozzle is mutated if the average velocity exceeds 4 m/s (13.1 ft/s). This is a second penalty function that removes infeasible designs from the product pool.

3.8 Evolutionary Algorithm Description

Figure 17 outlines the evolutionary algorithm used. The initial population is generated randomly in Step A using the technique outlined above and used to populate a graph structure in Step B. For each mating event, a tournament group of five nozzles is selected. The first member of the tournament group is selected randomly from the population in Step C. This first member also serves as the first parent. The other tournament group members are determined in Step D using the graphing technique. Once the tournament group members are selected, they are sorted from best to worst based on the fitness criteria. The two nozzles with the lowest fitness values are identified as the two children to be replaced using the crossover technique above.

The second parent is selected using a roulette technique in Step E. First, the fitness values of each nozzle in the tournament group except the first parent are summed together. A random value is chosen between zero and sum value. Then, the fitness value of each nozzle is subtracted from the random value. The nozzle whose fitness subtraction brings the random value less than zero is selected as the second parent. This technique still allows some randomness in the selection of the second parent. However, it provides a statistical

advantage to the nozzles with higher fitness since their larger fitness values are more likely to reduce the random value less than zero.

Once the two parents and two children are identified, the mating event can be completed in step F. A forward cross as described above is performed to replace the first child. If a cross cannot be performed, then the child is replaced by mutation. A backward cross is performed to replace the second child. If a cross cannot be performed, then the child is replaced by mutation. Crossover and mutation are described in detail in Section 3.9. After the children are created, they are evaluated using the CFD solver in step G until the convergence criteria are satisfied. Step H replaces the lowest fitness tournament members with the newly computed children. Lastly, the mating is incremented in step I, and the process is repeated.

At the conclusion of the 2000 mating events, the fitness value of each nozzle is summarized in a file, along with the coordinates of the horn to allow review of the results.

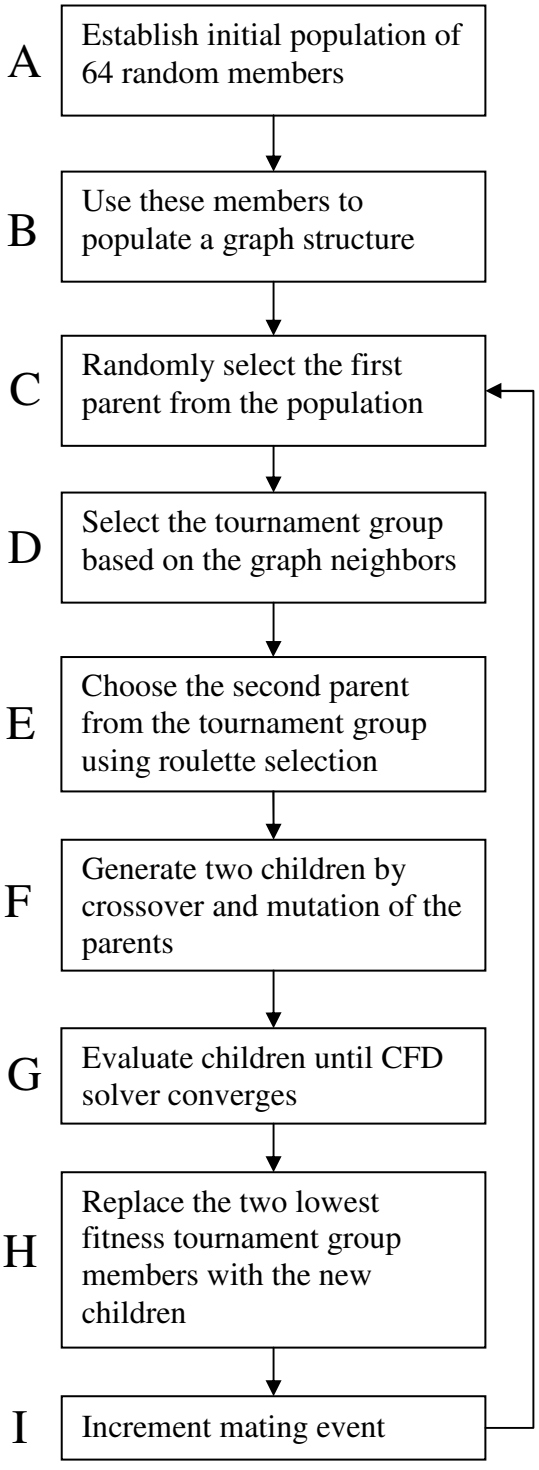

Figure 17. Evolutionary algorithm flowchart

3.9 Mating Event Detail

Figure 18 outlines the steps required to cross two nozzles. Before each mating event can occur, an analysis is performed to determine if a crossover can be performed. For two nozzles to be crossed, a minimum distance of overlapping geometry in the axial direction has to exist when one nozzle is superimposed over the other. Step 1 shows overlapping nozzles. For this work, the required overlap is 35.6 mm (1.4 in.). If two nozzles lack overlapping geometry, then they cannot be crossed. For a mating event of this type, a mutation would be performed. A mutation is defined as creating a brand new nozzle using the same technique outlined previously for creating the initial nozzle population.

This method of mutation results in a 100% penalty function in the algorithm. This may reduce diversity in the solution because any lower fitness child nozzles are simply replaced if the parents are too dissimilar. When this occurs, the diversity of design those nozzles held is lost and replaced by new geometry.

The crossover technique takes geometry from each of the parent nozzles and merges them to create two children. One nozzle is assigned to be the first parent, and the other the second parent. The first step is to select a crossover point. The crossover point is a randomly selected axial dimension in the overlapping range. An offset is applied to each end of the overlapping range to ensure that each nozzle has points on both sides of the crossover point. The offset used for this work was 12.7 mm (0.5 in.). The offset distances and acceptable crossover range are shown in Step 1. Step 2 shows a crossover point selected within the crossover range.

Once the crossover point is selected, the points defining the horn geometry are copied from each parent to the child. The first child is made by a forward crossover

operation. Points with an axial coordinate between zero and the crossover point are copied from the first parent into the child. Points with an axial coordinate greater than the crossover distance are copied from the second parent. Step 3 shows the geometry selected from each parent and its relationship to the crossover point.

A backward crossover operation copies the points for the second child. Points with an axial coordinate from zero to the crossover point are copied from the second parent, and points with an axial coordinate greater than the crossover point are copied from the first parent.

Once the points have been copied from each parent, the geometry must be merged at the discontinuity. To do this, a point is created with an axial coordinate equal to the crossover distance. The radial coordinate is determining by averaging the radial coordinates of the first point before the crossover distance and the first point after the crossover distance. Step 3 shows the crossover point. Sharp transitions between the horn pieces are avoided by checking the angle of each line segment in each direction from the crossover point. If the included angle between the radial axis and line segment is greater than forty-five degrees, the radial coordinate of the point is adjusted to bring the angle into specification. Each segment in each direction from the crossover is checked and adjusted until one is found within specification. The discontinuity check is performed to reduce numerical error, improve nozzle manufacturability, and produce well formed CFD grids. Step 4 illustrates the geometry smoothing technique. Once all the points have been copied and smoothed, a new horn outline can be created. The finished child horn is shown in Step 5.

Step 1:

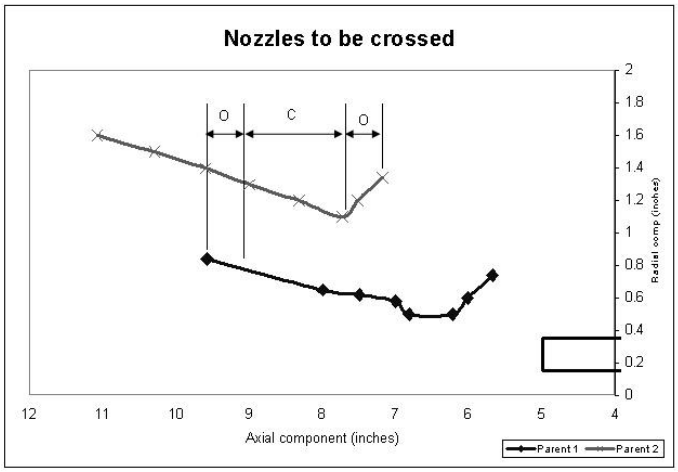

O = Overlap Offset Distance
C = Range in which cross point can

Step 2:

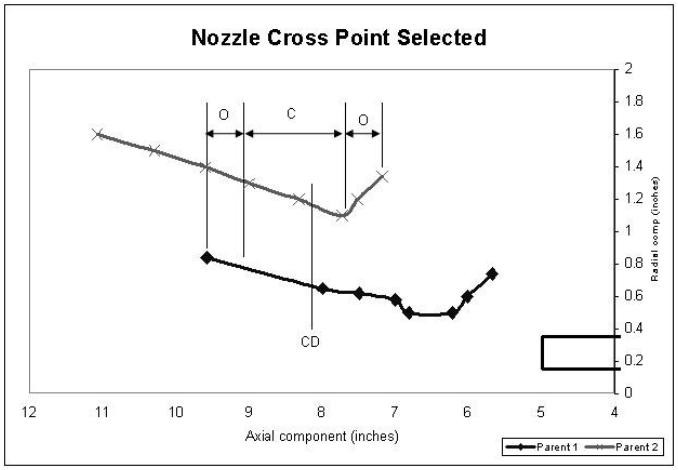

O = Overlap Offset Distance
C = Range in which cross point can be chosen
CD = Crossover distance, chosen at random in the defined range

Step 3:

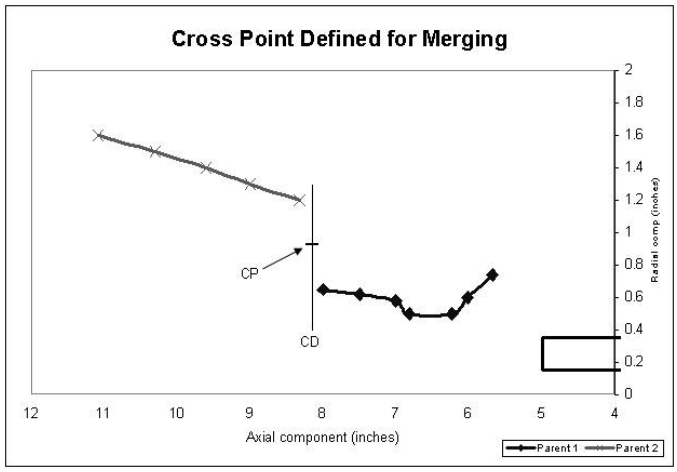

CD = Crossover distance
CP = Crossover point

Figure 18. Nozzle mating procedure. There are five steps to take a segment of geometry from each parent nozzle and combine them into a new child nozzle.

Step 4:

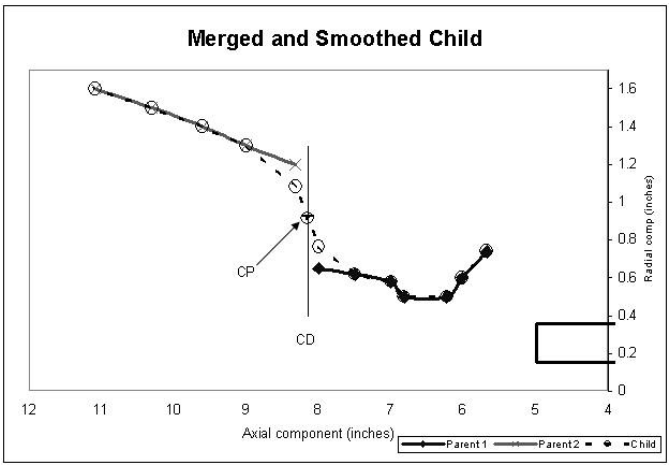

CD = Crossover point, chosen at random in the defined range

Step 5:

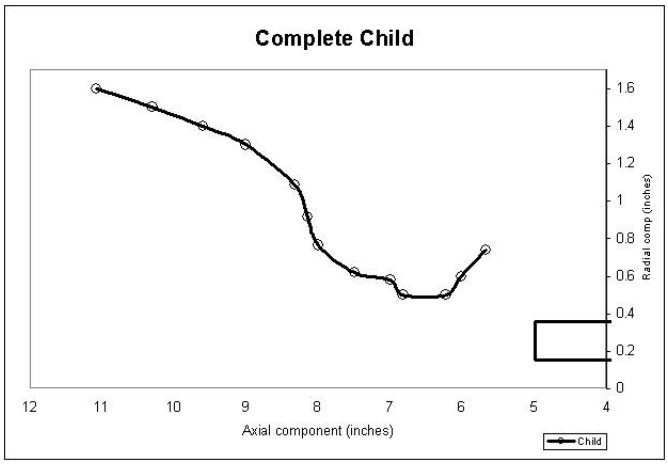

Figure 18. (continued)

CHAPTER 4

Results

To determine which designs represent an improvement over the current model, some benchmarks are necessary. The currently manufactured design has a fitness of 0.91 based on computed magnification ratio and velocity values from the highest fidelity model in the grid study.

Nozzles with a fitness value around 1.7 are created using the procedures described in this work. This is 87% higher than the nozzle commercially available. All types of EA graphs are able to produce nozzles with this performance. Table 3 summarizes nozzle performance and physical attribute data. Figure 19 graphically illustrates the nozzle outline and fluid velocity for eight computed solutions.

Review of the data in Table 3 shows that each of the nozzles in Figure 19 has very similar performance. The nozzles have some variation in their design, which can be observed through visual inspection and review of the tabular data.

All the nozzles have exit diameters very close to 12.7 mm (0.5”). This is the minimum diameter that the code is allowed to create. This diameter is such that a velocity profile without an excessive gradient is maintained across the outlet of the nozzle. An exit velocity profile with a low gradient across the exit allows for improved momentum transfer from the jet to the entrained fluid. The low gradient minimizes the peak velocity required for a specific momentum, and a lower velocity requires less power. This encourages the nozzle to combine entraining fluid with horn exit velocity to create a balanced design.

Combining the fitness evaluation with engineering experience allows the selection of more viable candidate solutions from the designs created by the algorithm.

Table 3: Nozzle performance summary

Nozzle	Fitness	Horn Exit Velocity (m/s)	Horn Length (mm)	Entrain Length (mm)	Entrance Diameter (mm)	Exit Diameter (mm)
C64_1	1.67	6.80	79.0	10.9	59.9	25.8
C64_2	1.71	6.89	106.2	8.4	51.8	25.4
H64_1	1.72	7.00	73.2	15.5	39.6	25.6
H64_2	1.64	6.39	107.4	23.1	47.8	25.4
P32_1	1.73	7.04	97.8	6.9	42.7	25.6
P32_2	1.70	6.76	102.4	14.7	30.5	25.6
T4_1	1.69	6.74	113.0	9.7	48.3	25.7
T4_2	1.66	6.62	130.3	5.8	69.6	25.8
Ref noz	0.91	2.51	99.1	17.3	37.6	42.7

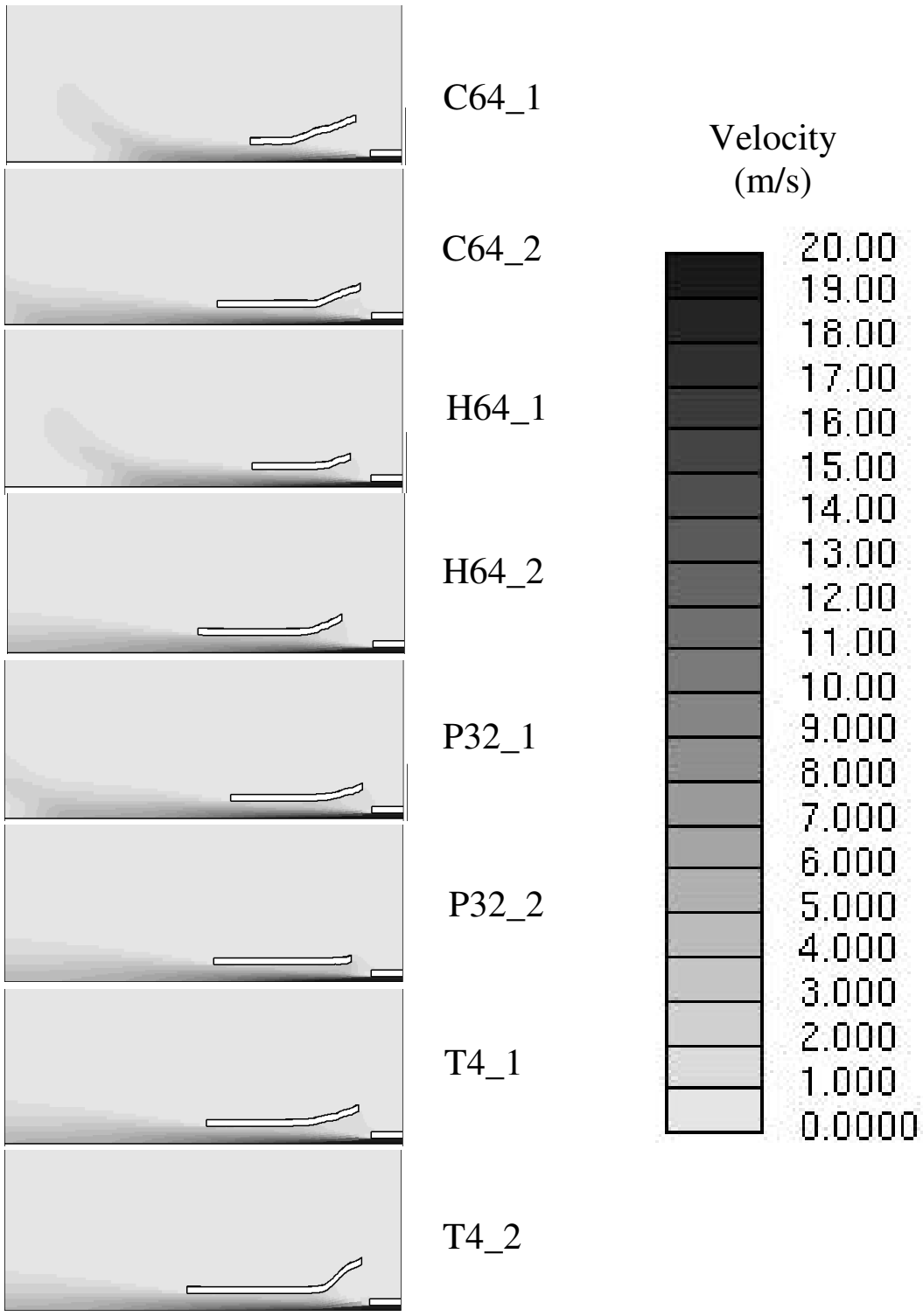

Figure 19. Evolutionary algorithm results. The two best nozzles from each of four graph types with their velocity contour plots are shown. Refer to Table 3 for nozzle geometric dimensions.

The lengths of the nozzles vary from 73 mm (2.88”) to 130 mm (5.13”). The length has limited effect on the nozzle outlet speed but some effect on the distance the higher velocity flow reaches from the nozzle. That is, longer nozzles can throw water farther from the end of the jet than the shorter ones.

The size and shape of the nozzle entrance is the most varied feature of the nozzle group reviewed. This is the zone where bulk fluid is entrained with the jet flow to enter the nozzle horn. Originally it was expected that nozzle performance would be very sensitive to this aspect of the design. The results shown here suggest the design may be more robust in this area than was expected. Some of entrances are wide, such as the C64_1, C64_2, and T4_2 nozzles that are shown in Figure 19, allowing a gentle entrance. Others are abrupt, such as P32_2. Each design entrains a similar amount of bulk fluid. The equivalent entrainment performance of each design perhaps suggests that simply a minimum size entrainment area is required for effective nozzle performance.

The above data contrasts with the production nozzle used as a benchmark, with a nozzle exit speed of 2.51 m/s, magnification ratio of 4.07, and fitness of 0.909. The computed nozzles perform much better with regard to nozzle exit speed. However, magnification ratio is reduced in order to accomplish this. The computed nozzles have a magnification ratio of 3.1 to 3.4. The engineer has the ability to consider the conditions specific to the mixing application and to emphasize the desired characteristics, such as nozzle throw, magnification ratio, or exit speed.

4.1 Evolutionary Algorithm Results

The torus and Peterson graphs generally create the highest-performing nozzle groups. These graphs create groups with average fitness values near 1.75 and 1.65, respectively. Inspection shows that the most obvious difference is, generally, the new nozzles do not widen as the end of the horn is reached. This appears to allow the jet to reach farther into the domain by maintaining high fluid velocity longer and more constant velocity across the horn exit.

Also of interest is the performance of the evolutionary algorithm as the mating events progress. The initial pool of nozzles used for the mating events is generated randomly using the process described earlier in this paper. Figure 20 shows the maximum, minimum, and average nozzle fitness for each mating event during a C64 graph experiment. The maximum performing nozzle is created during the beginning phase when the pool is populated. The algorithm never generates a nozzle with higher performance. However, the average performance is improved with time as the traits of the highest performing nozzles are integrated into the lower performing ones. The average performance becomes very near that of the best nozzle near the end of the mating sequence. This is because the other nozzles become more similar to the highest performing nozzle with each successive mating event. The other three graphs exhibit the same pattern of behavior, the only difference is that the average fitness rises more quickly than the illustrated sample data. Figure 21 shows the results from the hypercube. Figure 22 shows the results from the Peterson. Lastly, Figure 23 illustrates the results from the toroid.

The Peterson and torus graphs create the most nozzles of high fitness. The nozzles at the conclusion of each of these graphs are all similar to each other. Each of these graphs

changes the nozzle pool such that the average is very close to the maximum. These graphs also require fewer mating events to reach the maximum average than the cycle and hypercube graphs. These graphs have high levels of connectivity, which is created by larger tournament groups. Larger tournament groups allow each nozzle to have a larger number of possible mates, which allows high performing geometry to be spread more quickly. This raises the performance level of the population and creates more similarity among the member nozzles.

As the Peterson, hypercube, and torus graphs progress, the nozzle population become more homogenous. Figure 24 illustrates this conclusion. This figure plots the length of each nozzle horn in the population of a torus graph at each mating event. As the mating events progress, the nozzles converge on just one nozzle length. Inspections of other characteristics such as entrainment length reveal a similar pattern. This same performance can be noted on both the Peterson and torus graphs, as well. A review of the data from the C64 graph in Figure 25 shows a lower tendency to exhibit this trait. The nozzle lengths do consolidate as the algorithm progresses, but several lengths survive all the way to the end of the run. The fitness of each group that survives to the end is also noted.

The population size of the C64 and H64 runs are equal. The more significant homogeneity of the H64, P32-3, and T4-16 graphs causes the data points to consolidate at only two fitness values. These two fitness values correspond to two nozzle designs, and all the graph members consolidate to these two designs by the completion of the run. A conclusion on sensitivity cannot be reached from this consolidated sample.

Multiple runs of each graph are completed. Each graph type performs consistently. For examples, all Peterson graphs have maximum fitness near 1.67, and have similar slopes of average fitness.

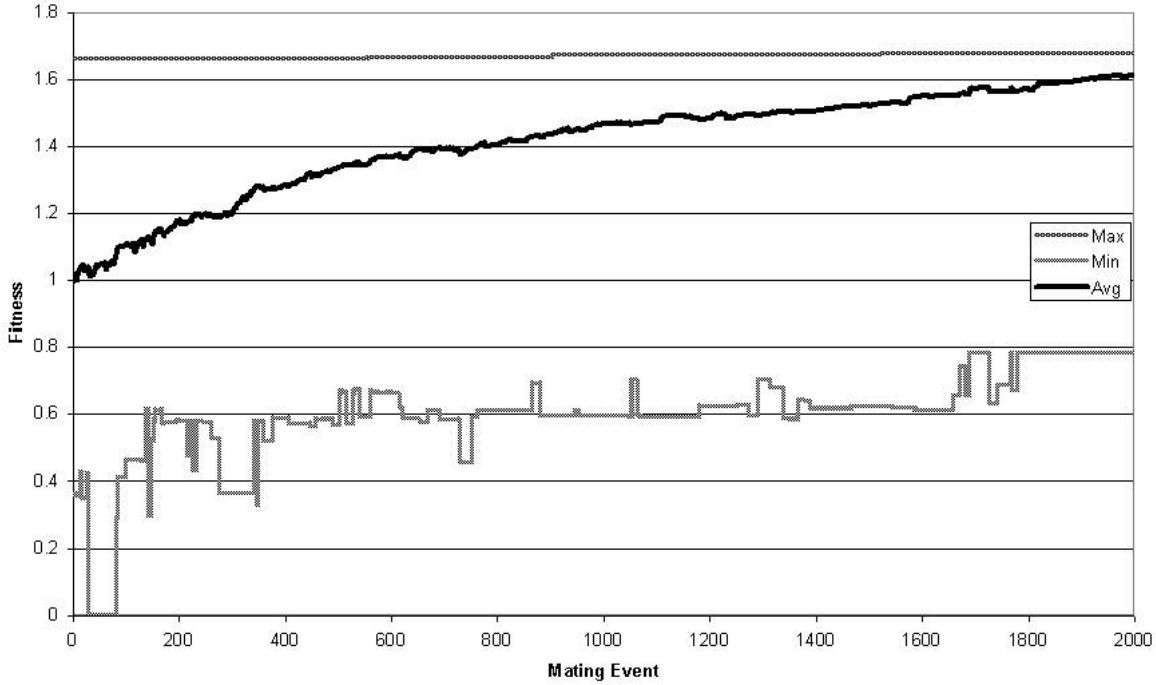

Figure 20. Fitness vs. mating event summary for the C64 graph structure

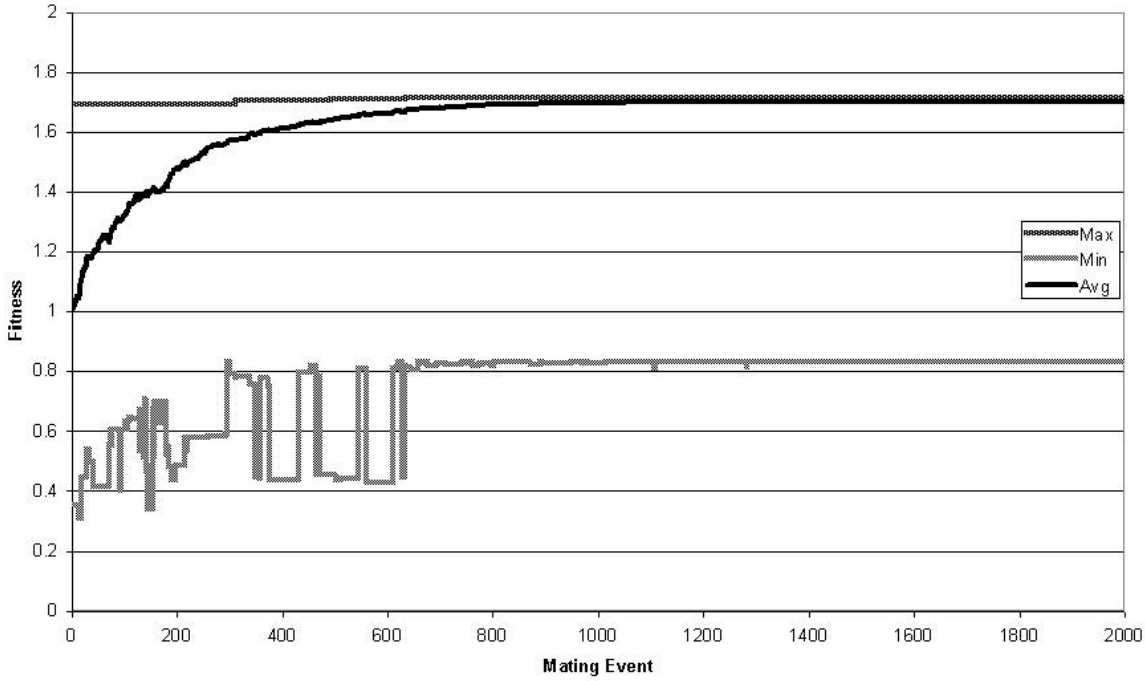

Figure 21. Fitness vs. mating event summary for the H64 graph structure

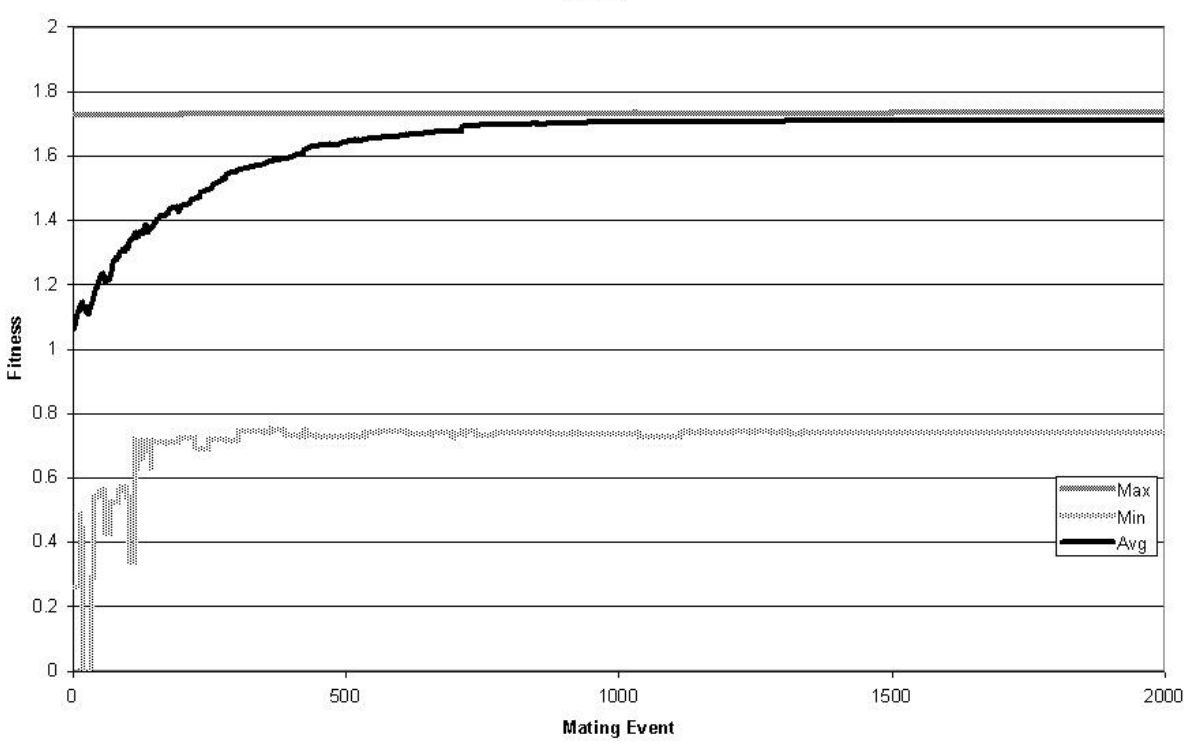

Figure 22. Fitness vs. mating event summary for the P32-3 graph structure

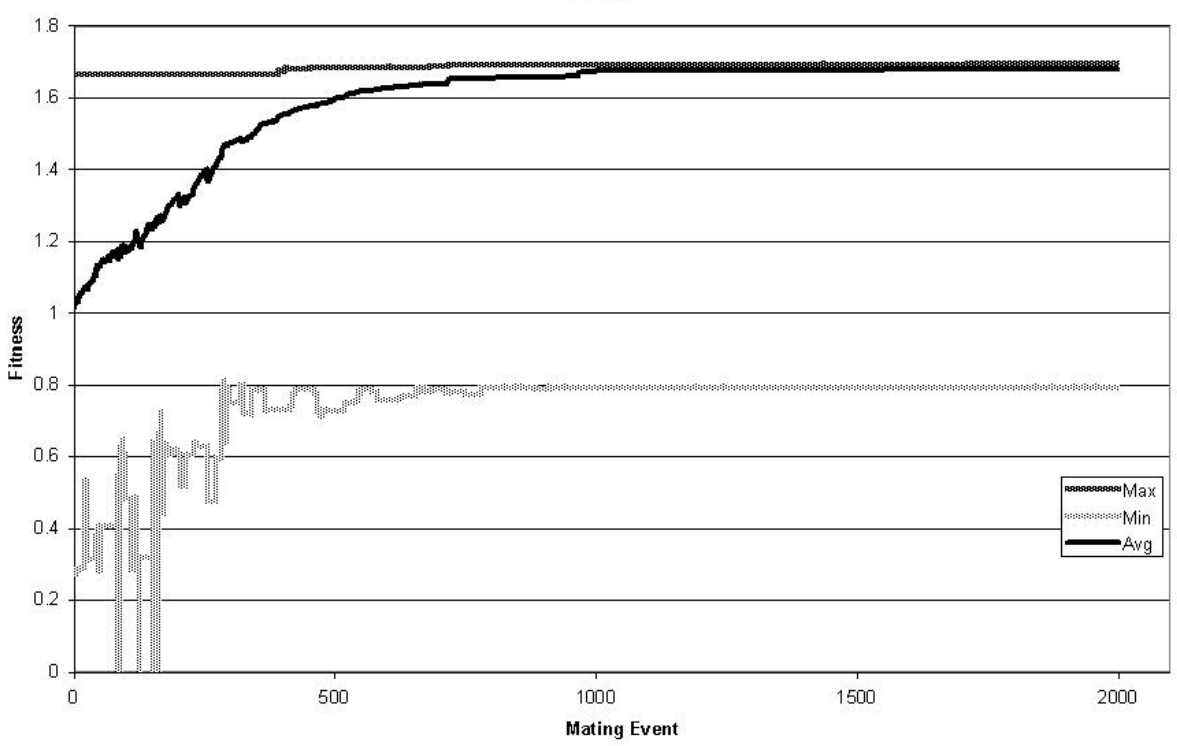

Figure 23. Fitness vs. mating event summary for the T4-16 graph structure

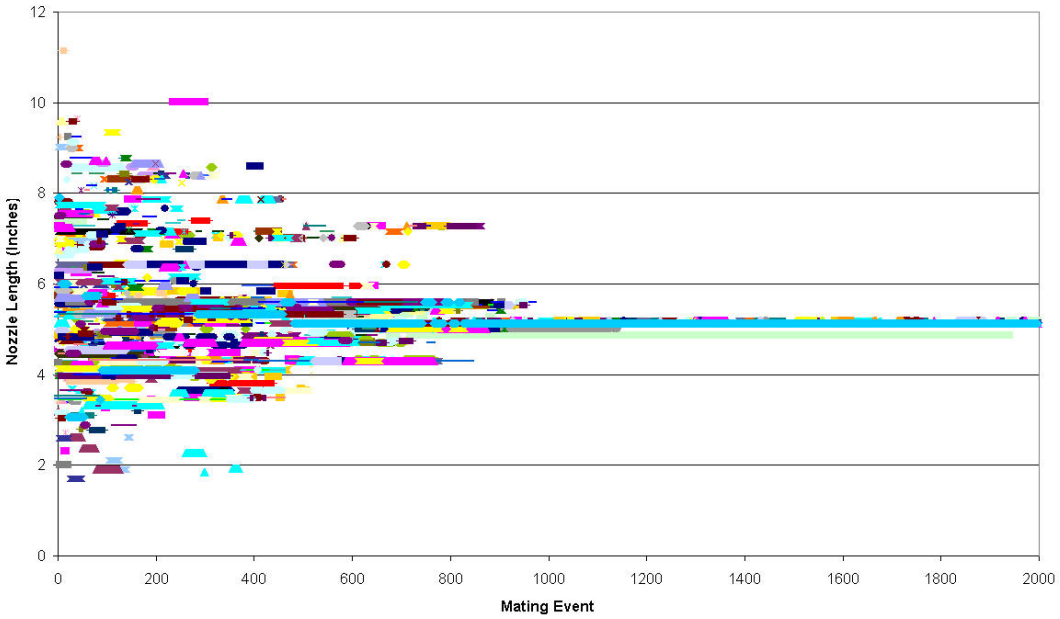

Figure 24. Nozzle length vs. mating event summary for the T4-16 graph structure. The fitness value is about 1.7 at the conclusion of 2000 mating events.

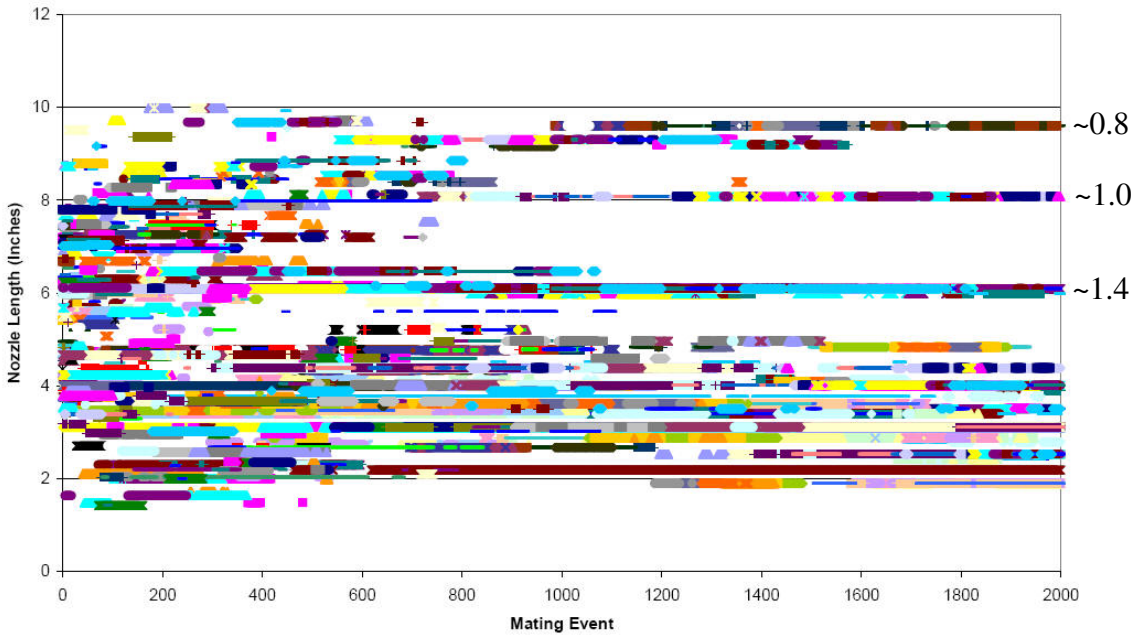

Figure 25. Nozzle length vs. mating event summary for the C64 graph structure. Fitness values are listed to the right for the distinct nozzle groups.

CHAPTER 5

Conclusions

This work demonstrates that it is possible to design a new nozzle that is better suited to the selected fitness criteria than the currently manufactured design. The algorithm and analysis tools developed allow repeated creation of a design pool with increased performance levels.

Comparing the computed designs to the manufactured designs shows that diameter is the most significant characteristic. The diameter of the computed nozzles is generally smaller than that of the manufactured nozzle. While increasing nozzle exit speed, some entrained flow, measured in terms of magnification ratio, is sacrificed. But, the higher exit speed allows the plume of high velocity fluid to extend farther into the domain past the nozzle, and this in turn extends the velocity gradient that causes mixing. In this way, the computed designs better satisfy the fitness criteria used for this work. The tools presented here could be used with modified fitness specifications to determine the nozzle required for an alternate mixing application.

The results show that the performance of the nozzle has limited sensitivity to the entrance geometry of the nozzle horn for this fitness parameter. Several varied entrance shapes result in nozzles with similar fitness performances. A different fitness parameter may show more coupling between nozzle performance and nozzle entrance size and shape.

It is important to note that the best design is present in the initial design pool of each graph run. No hybrid vigor exists for this type of design problem. This also suggests that perhaps higher performance levels could be reached if the randomly generated initial design

pool were replaced with a set of promising designs for the algorithm to use. Results consolidate into several groups when using the cyclic graph.

Further developments of the requirements for specific mixing applications would be a valuable addition to this work. The developed tool can be used to generate designs to meet a set of requirements. But, these results could be refined and improved further with a better understanding of the mixing requirements. Does an application require a slow, consistent mixing velocity, or several small jets with a high velocity gradient relative to the bulk fluid? Questions like these would require consideration of such things as tank size, number of mixing nozzles available, fluids and/or solids being mixed, hydraulic mixing flow available, and other factors as required. Nozzle discovery models could be sharpened with additional information such as this.

This algorithm can assist the design engineer by creating several choices that meet the specified criteria. Nozzles can be designed to meet needs such as a minimum flow projection distance or a maximum pressure drop. Different nozzle designs that all have the same performance criteria can also be located with this algorithm. This could allow searching for a design better suited for a specific manufacturing process with equal performance. Choices can give the engineer better insight into the characteristics affecting the design or performance, or allow the discovery of an improved solution governed by a specified set of constraints.

REFERENCES

Ashlock, D.A., Bryden, K.M., Corns, S., Schonfeld, J., 2006. An Updated Taxonomy of Evolutionary Computation Problems using Graph-based Evolutionary Algorithms. Evolutionary Computation, CEC 2006. IEEE Congress on 16-21 July 2006, pp. 96-103.

Bryden, K.M., Ashlock, D.A., Corns, S., Willson, S., 2005. Graph Based Evolutionary Algorithms. IEEE Transactions on Evolutionary Computation 10, 550-567.

Bryden, K.M., Ashlock, D.A., McCorkle, D.S., Urban, G.L., 2003. Optimization of Heat Transfer Utilizing Graph Based Evolutionary Algorithms. International Journal of Heat and Fluid Flow 24, 267-277.

Folsom, R.G., 1948. Jet Pumps with Liquid Drive. Chemical Engineering Progress 44, 765-770.

Gosline, J.E., O'Brien, M.P., 1934. The Water Jet Pump. University of California Publications in Engineering 3, 167-190.

Hilgers, A., Boersma, B.J., 2001. Optimization of Turbulent Jet Mixing. Fluid Dynamics Research 39, 345-368.

Mann, R., Pillai, S.K., El-Hamouz, A.M., Ying, P., Togatorop, A., Edwards, R.B., 1995. Computational Fluid Mixing for Stirred Vessels: Progress from Seeing to Believing. The Chemical Engineering Journal 59, 39-50.

Mann, R., Togatorop, A., Senior, P.R., Graham, P., Edwards, R.B., 1997. Evaluating Mixing in Stirred Reactors by 3-D Visualization: Partial Segregation for Dual Feed Semi-Batch Operation. Part A. Transactions of the Institute of Chemical Engineers 75, 755-762.

Mitchell, M., 1998. An Introduction to Genetic Algorithms. MIT Press, Cambridge, MA.

Reynolds, T.D., Richards, P.A., 1996. Unit Operations and Processes in Environmental Engineering. 2nd ed. PWS Publishing Company, Boston, MA.

Teigland, R., Eliassen, I., 2001. A multiblock/multilevel mesh refinement procedure for CFD calculations. International Journal for Numerical Methods in Fluids 36, 519-538.

Ucar, T., 1998. Simulation and Experimental Study of Jet Agitation Effects on Agrochemical Mixing in Sprayer Tanks. The Ohio State University, Columbus.

Ucar, T., Fox, R.D., Ozkan, H.E., Brazee, R.D., 2001. Simulation of Jet Agitation in Sprayer Tanks: Comparison of Predicted and Measured Water Velocities. Transactions of the ASAE 44, 223-230.

Yates, W.E., Akesson, N.B., 1963. Hydraulic Agitation Requirements for Pesticide Materials. Transactions of the ASAE. pp. 202-205,208.

Zughbi, H.D., Rakib, M.A., 2004. Mixing in a Fluid Jet Agitated Tank: Effects of Jet Angle and Elevation and Number of Jets. Chemical Engineering Science 59, 829-842.